Modelling and Simulation of Plasmonic Waveguides and Nanolasers

by

Haotong Wang

A Thesis Presented in Partial Fulfillment
of the Requirements for the Degree
Master of Science

Approved April 2014 by the
Graduate Supervisory Committee:

Cun-Zheng Ning,Chair
Hongbin Yu
Joseph Palais

ARIZONA STATE UNIVERSITY

May 2014

ABSTRACT

This thesis summarizes modeling and simulation of plasmonic waveguides and nanolasers. The research includes modeling of dielectric constants of doped semiconductor as a potential plasmonic material, simulation of plasmonic waveguides with different configurations and geometries, simulation and design of plasmonic nanolasers. In the doped semiconductor part, a more accurate model accounting for dielectric constant of doped InAs was proposed. In the model, Interband transitions accounted for by Adachi's model considering Burstein-Moss effect and free electron effect governed by Drude model dominate in different spectral regions. For plasmonic waveguide part, Insulator-Metal-Insulator (IMI) waveguide, silver nanowire waveguide with and without substrate, Metal-Semiconductor-Metal (MSM) waveguide and Metal-Insulator-Semiconductor-Insulator-Metal (MISIM) waveguide were investigated respectively. Modal analysis was given for each part. Lastly, a comparative study of plasmonic and optical modes in an MSM disk cavity was performed by FDTD simulation for room temperature at the telecommunication wavelength. The results show quantitatively that plasmonic modes have advantages over optical modes in the scalability down to small size and the cavity Quantum Electrodynamics(QED) effects due to the possibility of breaking the diffraction limit. Surprisingly for lasing characteristics, though plasmonic modes have large loss as expected, minimal achievable threshold can be attained for whispering gallery plasmonic modes with azimuthal number of 2 by optimizing cavity design at 1.55µm due to interplay of metal loss and radiation loss.

DEDICATION

This thesis is dedicated to my patents for their unconditional love and support for the past twenty five years.

ACKNOWLEDGMENTS

I would like to acknowledge my advisor Prof. Cun-Zheng Ning for introducing me in to this exciting field in his group. Not only do I get an opportunity to approach the frontier of scientific research but also benefit a lot from his broad knowledge and serious attitude towards research.

I want to thank all the group members in Dr. Ning's Nanophotonics Group especially Kang for his time to teach me how to conduct modeling and simulation by different methods. His in-depth understanding of physics concepts provides me a starting point to simulate the real world. I also would like to thank a previous member of our group Debin Li who specialized in this area and gave me many inspirations through his excellent work carried out previously.

Lastly and most importantly, I must thank my mother and my father for their endless love, support, faith and care.

TABLE OF CONTENTS

LIST OF FIGURES

vi

CHAPTER 1

PLASMONIC MATERIALS AND SURFACE PLASMONS

1.1 Plasmonic materials

Plasmonic materials offer an opportunity to explore plasmonic effects such as sub-wavelength guiding, field enhancement, small volume sensing and other nonlinear effects due to its unique optical responses. Efforts have been made constantly to look for new promising plasmonic materials to meet the ever-increasing demand in plasmonics- related applications. So far, potential plasmonic materials include noble metals, highly-doped semiconductors, transparent conducting oxides, metal nitrides and 2D graphene [1]. Here I only focus on two of them. One is conventional plasmonic materials, the noble metals such as Ag, Au, and Al. The other one is highly doped semiconductors which is a possible promising alternative aiming at different spectral region.

It is known that noble metals behave like perfect electric conductors in the low frequency range such as hollow metal pipe waveguide used for a microwave region. At the high frequencies, such as visible region of spectrum, metal behavior changes qualitatively. The well-known Drude model is widely used to fit the permittivity of noble metals in this range with an assumption that electrons are not bound, as shown below:

$$\varepsilon(\omega) = \varepsilon_\infty - \frac{\omega_p^2 \varepsilon_0}{\omega^2 + i\omega\gamma}$$

where ε_∞ is high frequency permittivity, ω_p is plasmon frequency, γ is collision rate. Typical value for gold are ε_∞ =9.5, ω_p =8.95eV, γ =0.069eV. Fig1.1 shows the plots of real and imaginary parts of gold over the range from visible to near infrared using the above parameters and compare with experimental Johnson & Christy data. It shows a good agreement with

experimental data. However, it should be noted that as wavelength decreases further below

600nm for gold, the imaginary part of permittivity deviates far from the experiment data due to

occurrence of interband transitions. So the Drude model is valid only at a certain region. To

model permittivity across the whole region, other factors such as interband transition and phonon

absorption should be considered.
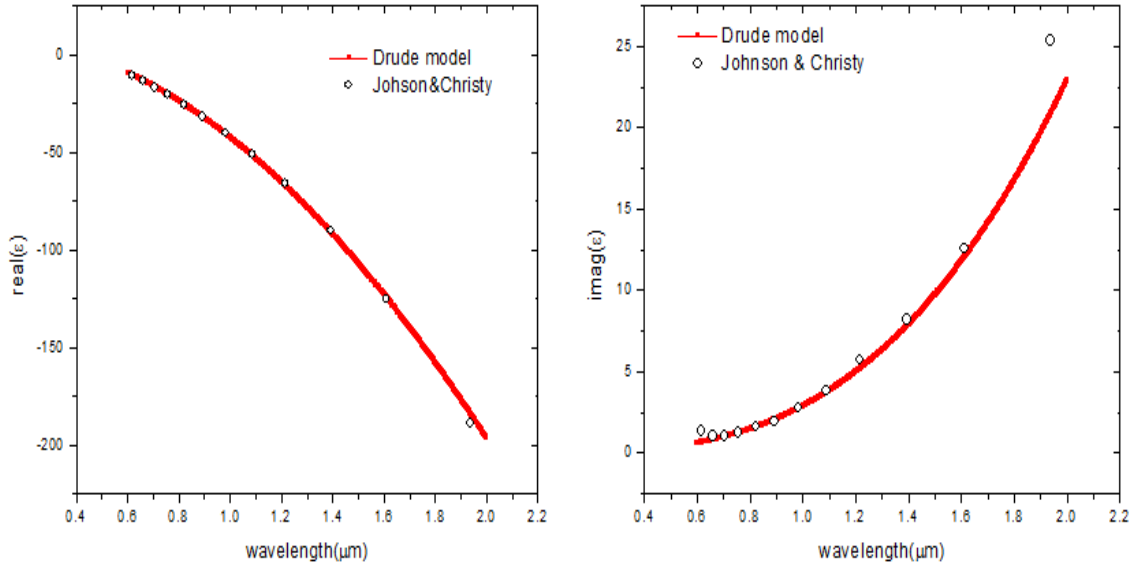
Fig1.1 Drude model fitting for gold compared with experimental data. Drude model (Red solid
curve) Experiment data (white dots)

Another model people often use for describing metal is the Lorentz model. Electrons in

metal are bound by a restoring force with a resonant frequency in the Lorentz model. So extra

parameter resonant frequency ω_0 is added in the expression below to describe plasma as a classic

harmonic oscillator:

$$\varepsilon(\omega) = \varepsilon_\infty + \frac{\omega_p^2}{(\omega_0^2 - \omega^2 - i\gamma\omega)}$$

where other parameters are the same as Drude model. Typical values for silver is ε_∞ =2.6,

ω_p =9.06eV, γ =0.02eV, ω_0 =0.079eV.The real and imaginary parts of silver permittivity as a

function of wavelength is shown below in Fig1.2. Again like Drude model, it shows decent

agreement with experimental data over the range from 600nm to 2000nm. However, here I only use tail part of Lorentz model to fit a certain range of permittivity by setting a low resonant frequency. So the interband transitions which take place in high frequency range are not considered here.
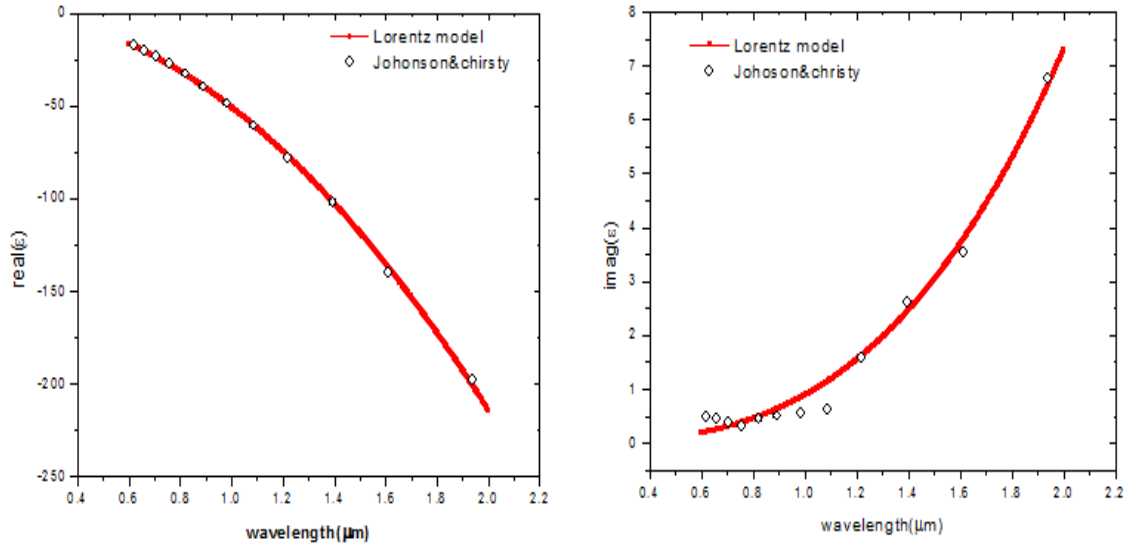
Fig1.2 Lorentz model fitting for silver compared with experimental data

To fully capture the optical response in the wide range, a combination of these two, the Lorentz-Drude model was frequently used by people. In the model, the Drude model and the Lorentz model account for the free electrons effect and interband transition respectively. The Drude-Lorentz model is given by the following equation:

$$\varepsilon(\omega) = 1 - \frac{f_0\omega_p^2}{\omega(\omega - i\Gamma_0)} + \sum_{j=1}^{k} \frac{f_j\omega_p^2}{(\omega_j^2 - \omega^2) + i\omega\Gamma_j}$$

where ω_p is plasmon frequency, Γ_0 and f_0 are damping constant and strength associated with free electron model, k is the number of oscillators with frequency ω_j, strength f_j and damping constant for Lorentz model. It is important to note here that the model should be carefully chosen depending on what range of wavelength you are interested in. For example, although the full

3

model can give me a good fitting across the whole range, I will use the simple Drude model for most of my simulation in the thesis since no interband transitions happen in my wavelength interest. For some other part of my simulation, interpolation of experimental data is used for describing wavelength dependent of silver permittivity.

However, there are some drawbacks for metal being a perfect plasmonic material. Single wavelength range of plasmonic resonance, incompatibility with semiconductor manufacturing process and high metal loss limit it for being an ideal building block in a plasmonic-based system [2]. To avoid these intrinsic disadvantages, efforts on finding new substitutes never stop. Doped semiconductor is probably one of those substitutes, because the complex permittivity of it is very similar to that of the metal at near optical frequency, except that the effective mass of the electrons for the n-type doped semiconductors or the holes for p-type doped semiconductors have to be used [3]. By increasing the doping concentration, the optical response of highly doped semiconductor can behave like metal at a desirable wavelength range. Typically, for III-IV heavily doped semiconductors, metallic behavior happens at mid infrared range depending on achievable doping concentration. Thus, it is interesting to investigate the optical response of doped semiconductor for possible plasmonic application. Here I use a combination of Adachi's model and Drude model to analyze the permittivity of heavily doped InAs with different doping concentrations. The Adachi's model [4] which adopted critical points transition approach was applied here to account for interband transitions while the Drude model is responsible for the free carrier effect. The expression for permittivity is given:

$$\varepsilon_r(\omega) = \varepsilon_b - \frac{\omega_p^2}{\omega^2 + i\gamma\omega}$$

where $\omega_p^2 = \dfrac{Nq^2}{m^* \varepsilon_0}$, ε_b is dielectric constant related to interband transition, which as mentioned

earlier can be calculated by the Adachi's model. It should be noted here Adachi's model is only

valid for lightly or undoped semiconductor. To fully consider the effect of doping on the

absorption, $\alpha = \alpha_0 (f_v - f_c)$ is used where α and α_0 represent absorption coefficient for heavily

doped and undoped semiconductor respectively. f_v, f_c are the Fermi-Dirac distributions for the

electrons in the valence band and in the conduction band. Usually the values of f_v, f_c are set to be

1 and 0 for undoped semiconductor as the valence band is completely occupied and the

conduction band is empty. For highly doped semiconductors, the case is different as the

absorption edge is pushed to higher energy due to populated state at the bottom of conduction

band, which is a famous phenomenon called Burstein-Moss effect. The $f_v - f_c$ as a function of

energy for InAs at different doping concentrations are shown in Fig1.3. Clear band gap shift can

be observed from the figure. After considering the doping effect on the absorption, α is

connected with the imaginary part of dielectric function by $\varepsilon_2 = \dfrac{\alpha n_b c}{\omega}$ where c is speed of light

and n_b is the background refractive index. For the Drude model part, the parameters are adopted

from experimental data [5] measured by UIUC group. Until now, the whole dielectric function

model has been proposed and results are shown in Fig1.5 and Fig1.6. As can been from the

figures, each contribution part dominates at different spectral regions. At Mid IR region, free

electrons effect contributes most such that real part of permittivity can reach negative .From

Fig1.4, tunability of transition energy for real part of permittivity becoming negative is shown.

This doping dependent relationship enables people to explore plasmonic effect of highly doped

semiconductor at a desirable wavelength range if assuming any effective heavy doping level is

achievable. As can be seen in Fig 1.5 corresponding to imaginary part of permittivity, free electrons model dominates first at longer wavelength and then interband transition takes over when energy is approaching or greater than band gap energy.
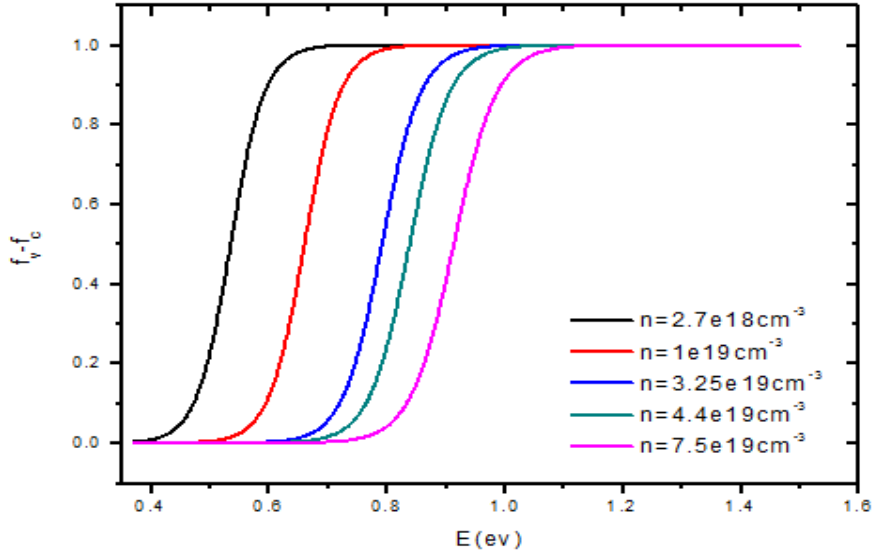
Fig1.3 fv-fc with respect to energy for different doping levels
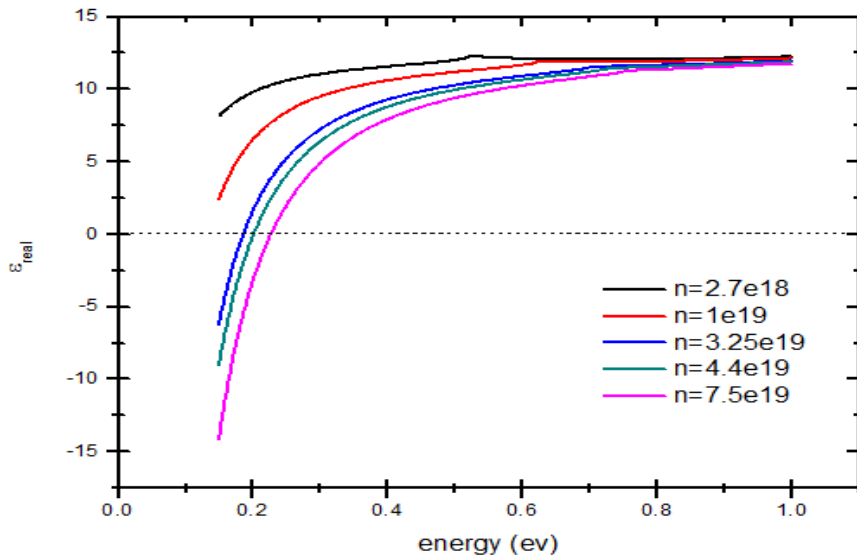
Fig1.4 simulated real part permittivity of InAs for different doping levels
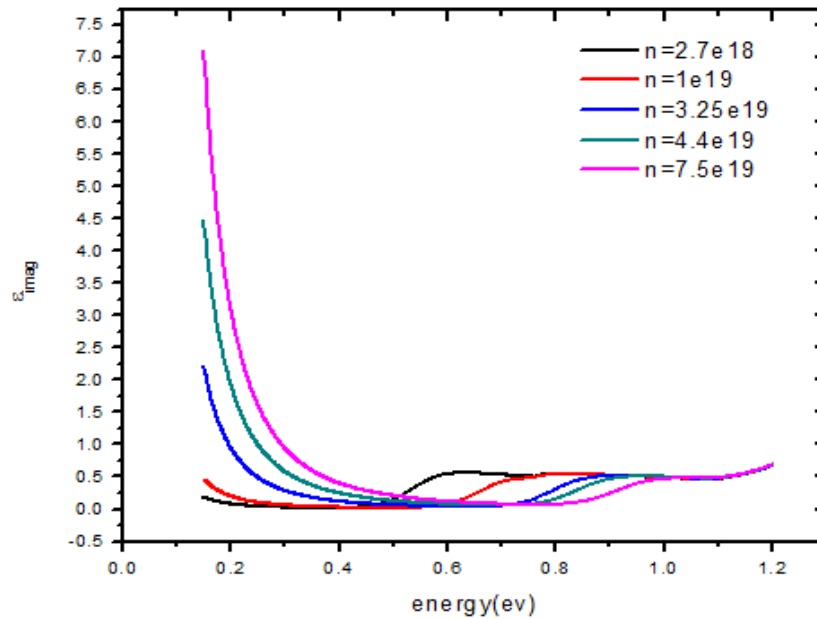
Fig1.5 simulated imaginary part permittivity of InAs for different doping levels

Tunability of plasmon wavelength within mid IR range and easy integration with semiconductor fabrication process make highly doped semiconductor a supplementary candidate serving as building block for plasmonic structure. However, a challenge remains as ultra high doping is typically difficult for semiconductor due to limited solubility for dopants as well as inefficient doping when doping level is high. The problem still remains to be solved but good news is GaN has been demonstrated to achieve a ultra high doping level of $3*10^{21}$ cm^{-3} [6]which holds some promise for replacing metal as alternating material even in NIR range.

1.2 Localized surface plasmon

Localized surface plasmon is an unique phenomenon formed by interaction between light and induced electrons oscillations in noble metal nanoparticles. The resonance is established at where the frequency of light matches with the natural oscillation frequency of surface electrons distributed on the metal called localized surface plasmon resonance. At resonance, the near field EM field is enhanced around the metal nanoparticle while in the far field the particle's extinction

7

spectrum has maximum peak due to cancellation of induced field and incoming field. To investigate how the EM field near the metal is enhanced, a simulation on the three silver nanoparticles system is performed by CMOSOL Multiphysics 4.2a. For a better comparison, pure dielectric systems with different permittivity which adopt an index confining mechanism are given as a contrast shown in Fig1.6.The incident light is from the top with polarization parallel to inter-particle axis with amplitude of 1 V/m.
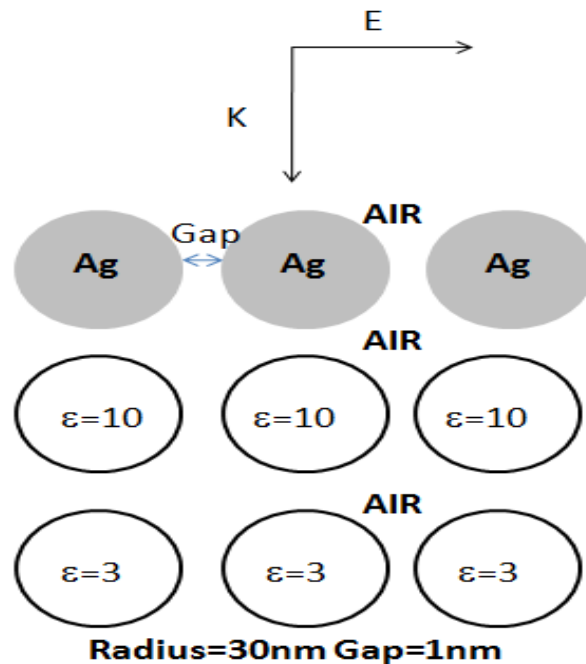
Fig1.6 Three different configurations for field enhancement study

The maximum field intensity inside the system with respect to wavelength is shown in Fig.1.7. Red and black curves stand for pure dielectric nanoparticles system with different dielectric constants while green curve is for metallic one. The peak of it represents where the resonance is with inset showing the field distribution at resonance. As can be seen from the figure, the metallic plasmonic system is far superior to conventional dielectric system in ability to enhance field whether it's on resonance or not. This great enhancement of field by metal

8

nanoparticles can find application in biosensing, especially in the Surface Enhanced Raman scattering (SERS) technique.
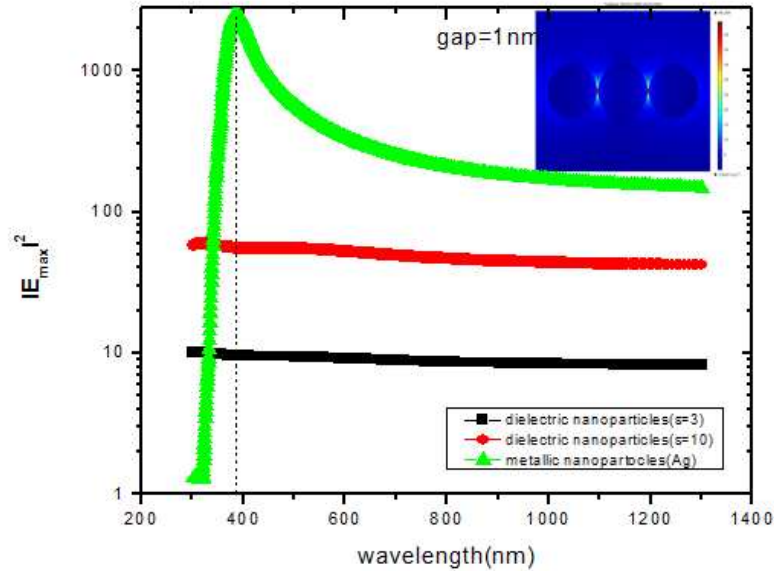
Fig1.7Maximum field intensity for different configurations with respect to wavelength Green color represents metal particles, Red color represents dielectric particles with permittivity of 10 and black color stands for dielectric particles with permittivity of 3.

Another method to determine the Localized surface plasmon resonance is to calculate the extinction spectral in the far field for metallic nanoparticles. The resonances occur at where the extinction spectral peaks. The Lumerical software based on FDTD simulation is used to investigate the optical response of metallic particles. Extinction cross section, scattering cross section and absorption cross section are calculated by the software for single gold nanoparticle in Fig1.8.Here the scattering cross section is defined as collected power in the far field normalized by intensity of incident light and absorption cross section is calculated by total power absorbed by particle in the near field divided by incident intensity, then the extinction cross section is a sum of these two. As can be seen from figure, local surface plasmon resonance occurs at around

9

500 nm for gold particle with a size of diameter 50nm and inset shows near field distribution at resonance. It's interesting to note that absorption process dominates for small size one as most of light is absorbed rather than scattered due to much smaller diameter than the wavelength of light. The following figure 1.9 gives the same plot but for gold dimmer with a 10 nm separation. Here it's worth to point that LSPR of nanostructure depends on a lot of factor such as shape, size, aspect ratio of structure and embedding environment.
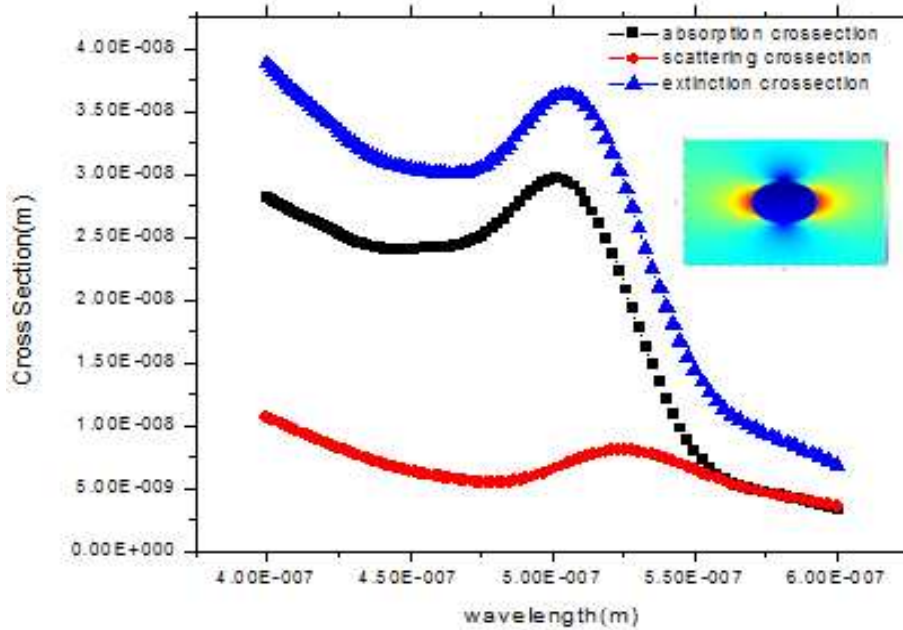
Fig1.8 Scattering (red) absorption (black) and extinction cross sections (blue) for gold particle with a diameter of 50nm .The inset shows field profile on resonance.
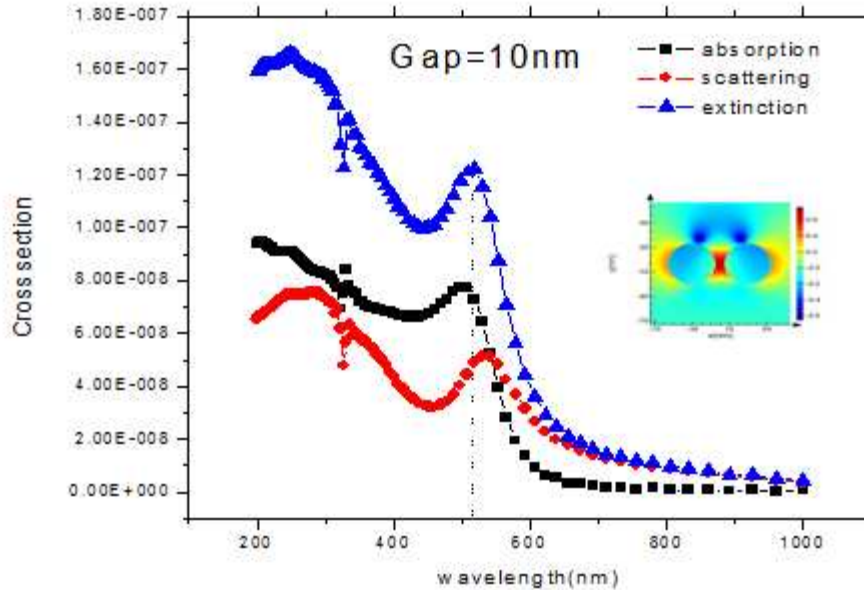
Fig1.9 Scattering(red) absorption (black) and extinction cross sections (blue) for gold dimer with gap of 10nm .The inset shows field profile on resonance.

Due to its high field enhancement and ability to focusing field in to a small volume, Localized surface plasmon resonance has found its application in biosensing technique such as Surface Enhanced Raman Scattering (SERS). Another advantage is tunable resonance of structure gives us more freedom to maximize the field enhancement. However, given the stochastic nature of nanopartice aggregation, it's difficult to track those "hot spots", which makes experiment uncontrollable and hard to replicate, So more attention has been paid to highly ordered, complex metallic system to exploit LSPR in a more controllable way.

1.3 Propagating surface plasmon

Propagating surface plasmon is the collective electrons oscillations coupled in to electromagnetic field, which propagate along the interface between metal and dielectric. The electric field is confined at the interface and decay along the two sides. To get a deep understanding this kind of mode, we would better start from Maxwell equation for a simple single interface case. A surface plasmon mode propagating along a single metal-dielectric

11

interface is shown in Fig 1.10.Actually in order to be supported by this structure, the surface plasmon mode has to be TM mode in nature with (Ex,Hy,Ez) components.
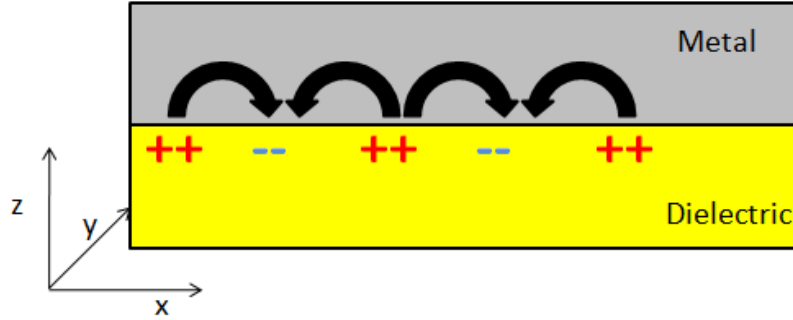
Fig1.10 surface plasmon polariton propagates along the single Metal-Dielectric interface

The electric and magnetic fields for a surface plasmon polariton which propagates along the x direction and decays along the z direction must take the following form:

$$H_d = (0, H_{yd}, 0)e^{i(k_{xd}x + k_{zd}z - \omega t)}$$

$$E_d = (E_{xd}, 0, E_{zd})e^{i(k_{xd}x + k_{zd}z - \omega t)}$$

$$H_m = (0, H_{ym}, 0)e^{i(k_{xm}x + k_{zm}z - \omega t)}$$

$$E_d = (E_{xm}, 0, E_{zm})e^{i(k_{xm}x + k_{zm}z - \omega t)}$$

where subscripts d,m represent dielectric and metal respectively, k_{zd}, k_{zm} means z component of wavevectors at dielectric part and metal part, $k_{xd} = k_{md} = k_x$ stands for x component of wavevector along the interface. By matching the boundary conditions in which Hy and Dz are continuous and substituting field equations in to Helmholtz equation $\nabla^2 \vec{E} + k^2 \vec{E} = 0$, we obtain the following relation:

$$\frac{\varepsilon_m}{k_{zm}} = \frac{\varepsilon_d}{k_{zd}}$$

$$k_x^2 + k_{zi}^2 = \varepsilon_i \frac{\omega^2}{c^2}$$

12

where i denotes either metal part or dielectric part, ε is permittivity of medium, ω means angular frequency of light, c is the speed of light. Combing those two equations, the dispersion relation of surface plasmon polariton can be given:

$$k_x^2 = k_0^2 \frac{\varepsilon_m \varepsilon_d}{\varepsilon_m + \varepsilon_d}$$

$$k_{zi}^2 = k_0^2 \frac{\varepsilon_i^2}{\varepsilon_m + \varepsilon_d}$$

The fig1.11 shows energy dispersion of surface plasmon polariton for silver–air interface. Red curve means analytic results which agree pretty well with simulation results represented by white dots. As can be seen from the figure, the propagating wavevector increase massively when energy increases, which means the effective wavelength propagating along the interface decreases correspondingly at high energy. At some point where the wavevector attains the maximum, the surface plasmon resonance is achieved. One thing not shown but should be noted that if increasing the energy further ,the dispersion curve would reflect back to small wavevectors region due to ohmic loss present in the metal.
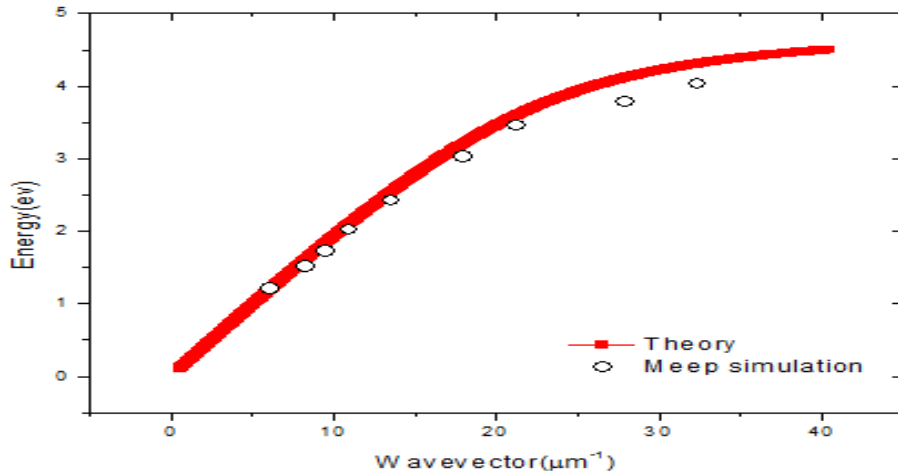
Fig 1.11 Energy dispersion relationship of surface plasmon for single Ag-air interface

As discussed above in the single interface case, wavelength in the medium can be shrinked massively in the propagation direction, which opens a possibility to squeeze light

energy in a very ultrasmall area. Another important structure supporting propagating surface

plasmon called Metal-Semiconductor-Metal (MIM) structure. MIM, as name indicates, consists a

dielectric core sandwiched by two metal slab given in Fig1.12.The propagation direction is along

x direction.
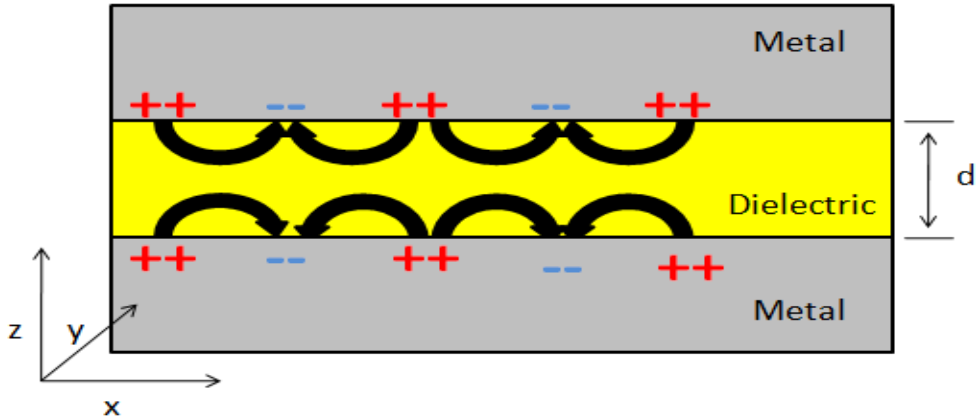
Fig1.12 Surface plasmon polariton propagates in MIM waveguide (symmetric case)
 Actually we can view it as two single metal-dielectric cases interacting with each other.

When d is too large for two surface plasmons to interact, no coupling effect happens. As d is thin

enough, then interaction between two single interface surface plasmons occurs. The smaller

distance between two metal slabs, the stronger interaction it has. The effect of interaction would

lead a splitting of mode in to two .one is symmetric mode, the other is antisymmetric one with

different phases of charge oscillation distributed on the metal surface. Here the symmetry is

defined as Ez with respect to the middle of dielectric layer. It's worth noting that although two

kinds of modes exist in this structure, it's difficult to excite antisymmetric mode in the real

practice due to field symmetry. Thus, we discuss only the symmetric case hereafter. The 2D

FDTD simulation was performed on this structure with uniform in the y direction. A dipole was

put at the entrance of MIM to excite plasmonic mode and d was set thinner than 100nm for

strong interaction. The dominant electric field Ez and magnetic field Hz distribution is shown in Fig1.13.The thickness of dielectric layer here is 20 nm.
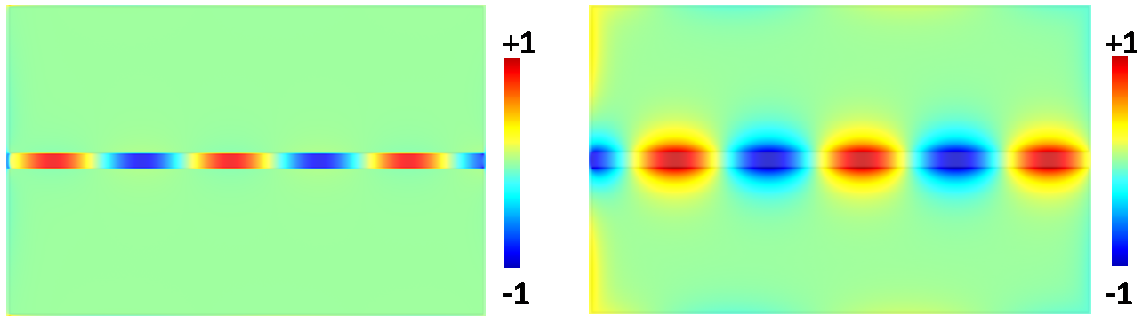
Fig1.13 Ez field distribution (Left)and Hy field distribution(right) for symmetric mode

As can be seen from the figure, the field energy is squeezed in to thin dielectric region with thickness far below the diffraction limit, which opens a possibility to realize subwavelength guiding utilizing this mode. To further understand the property of this mode, the energy dispersions for different thickness and different dielectric medium are given respectively in Fig1.14 and Fig.1.15.All of the curves asymptotically approach some certain energy values just like single interface case does, which is actually a common feature for energy dispersion of surface plasmonic mode. Those certain values correspond to different resonance energy of modes. From Fig1.14, as the thickness of dielectric decreases from 20nm to 5nm, the dispersion curve becomes flat meaning that the smaller wavelength of plasmon can be obtained for the same free space wavelength in the thinner waveguide (dielectric region). That's understandable since the interaction is much stronger in thinner one, leading a further exploration of plasmonic effect in the waveguide. In theory, the thickness can be indefinitely small and good news is current technology has enabled deposition of nanometer-thick film. Miyazaki [7] has achieved experimentally to squeeze visible light in to 3nm thick nanocavity with this kind of mode, which proved that utilizing plasmonic mode to achieve ultra-small nanocavity was feasible. In Fig1.15, dispersion curves for different dielectric mediums are given. As clearly can be seen, the

resonance energy for high index medium is lower that for low index one and MIM with high index core can enable better shrinking of light in visible wavelength range. As a consequence, much attention has been paid in to metal-semiconductor-metal structure with both gain available and high compression of light to achieve active waveguides and lasers.
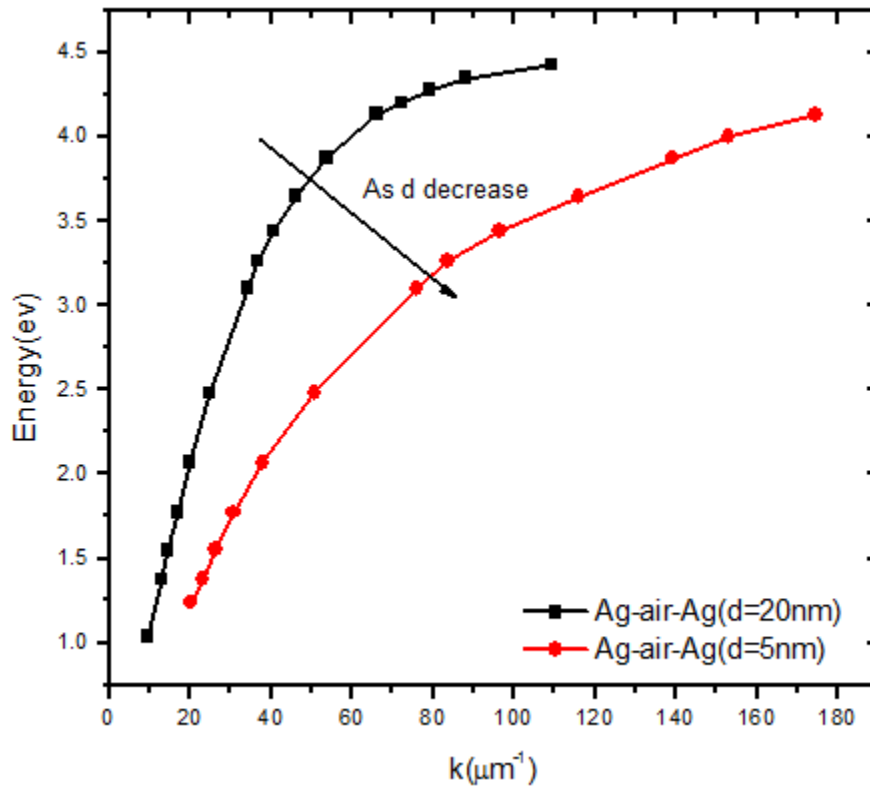
Fig1.14 Energy dispersion of symmetric plasmonic MIM mode at different thickness
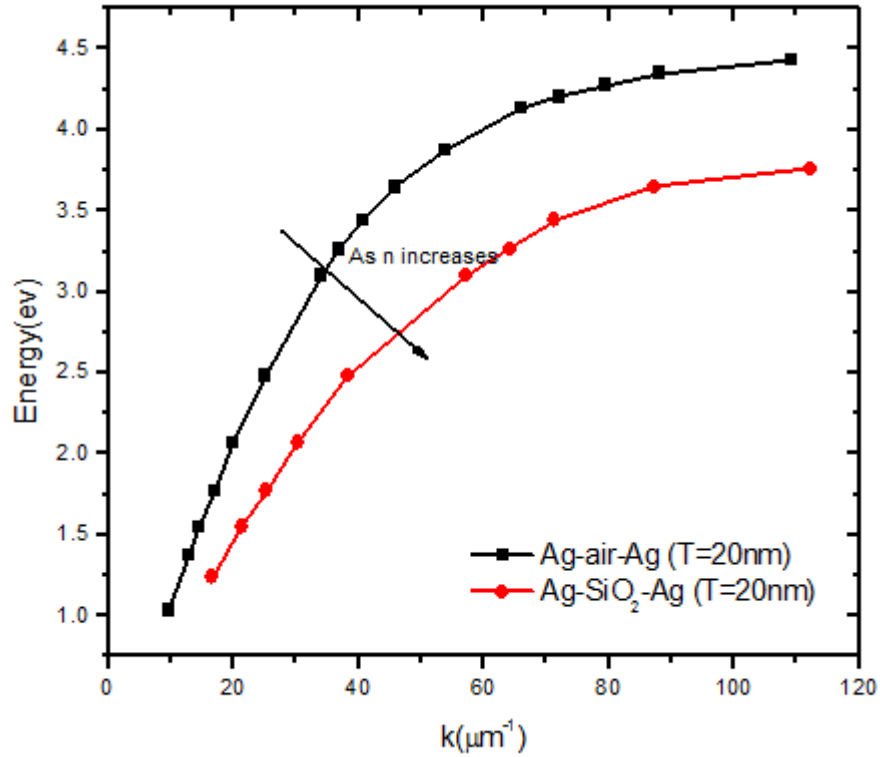
Fig1.15 Energy dispersion of symmetric plasmonic MIM mode with different cores

1.4 Summary

In summary, optical responses of two kinds of plasmonic materials-conventional noble metal and doped semiconductor are introduced. For doped semiconductor, a full dielectric function model including Drude model and modified Adachi's model considering Burstein-Moss effect was proposed. After that, basics of two surface plasmons including localized surface plasmon and propagating surface plasmon are given. The unique properties such as small modal volume, enhancement of electric filed, subwavelength confinement make them a potential candidate for miniaturization of photonic devices and investigation of light-matter interaction.

CHAPTER 2

PLASMONIC WAVEGUIDES

2.1 Insulator-metal-insulator waveguide

The plasmonic waveguide is a potential candidate for future chip communication due to subwavelength confinement far beyond the diffraction limit, which enables its integration with electronic transistors. Thus, numerous plasmonic waveguides with different configurations utilizing surface plasmon polariton attract people's interest. Of them, two prototype planer structures which are the metal film (Insulator-metal-insulator) and the metal gap (metal-insulator-metal) waveguide receive more attention than others due to suitability for nano-optical integrated circuits [8,9].The structure of IMI is given in Fig2.1.
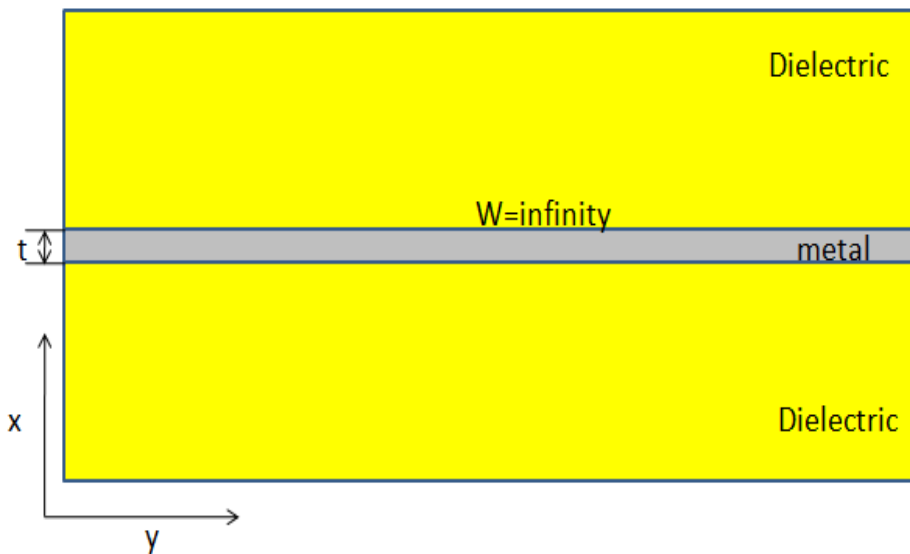
Fig2.1The cross section view of metal film embedded in dielectric

Fig.2.1 shows a cross section view of an infinite metal film embedded in the dielectric environment and propagation is along the direction perpendicular to the paper. Suppose the superstrate is the same as substrate, then this structure supports two kinds of modes, as MIM waveguide does. One is symmetric mode, which is also called Long-Range Surface Plasmon

Polariton (LRSP). The other mode is antisymmetric, namely Short-Range Surface Plasmon Polariton (SRSP). The symmetry here is defined with respect to Ex field. As name indicated, the LRSP has longer propagation length than the SRSP mode. It should be noted here that LRSP doesn't exist if the substrate is different from the superstrate due to break of symmetry. The Ex field distribution of two kinds of modes with metal thickness of 20nm at communication wavelength 1.55um is shown in Fig2.2.Here the silver is embedded in the dielctric(SiO_2)in the simulation.
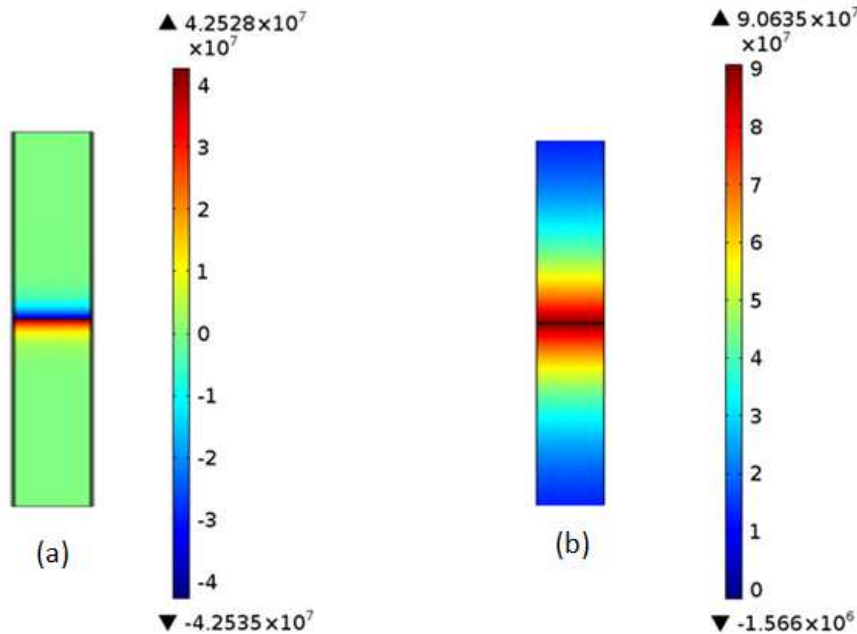
Fig2 .2 Ex field distribution for (a) SRSP and (b) LRSP

The effective index of two modes with respect to metal thickness at 1.55um is given in Fig2.3. As can be seen from the figure, when the metal thickness is relatively large, two surface plasmons propagate along each interface separately without interaction. So the effective refractive indexes for SRSP and LRSP are identical. As the thickness decreases, surface plasmons couple with each other , which leads to a splitting of mode in to the symmetric and

antisymmetric one. The upper branch, representing the antisymmetric mode, increases dramatically with the decreasing thickness while the lower branch approaches the permittivity value of dielectric, meaning the propagating mode is still bound at interface. Both of them show no cutoff with respect to thickness of the metal layer. As can be seen from Fig2.2, the SRSP mode is tightly bound to the metal surface, which results in a stronger modal confinement than that of LRSP. This point can also be reflected in increasing effective refractive index for SRSP in the Fig2.3. In order to compare two kinds of modes in transmission characteristics, the propagation loss of each mode is shown in Fig2.4. The propagation loss of SRSP dramatically increases with the decreasing thickness, while that of LRSP decreases massively showing itself a potential candidate for chip communication. Combined with results obtained from Fig2.3, we can conclude now SRSP has a strong confinement with a short propagation length whereas LRSP owns a long propagation length but with poor modal confinement. Although we can't combine these advantages into one mode, we can selectively excite either mode we prefer to use according to different applications. For example, we can use SRSP for nano-focusing or nano-guiding to confine light energy in to ultra-small area and adopt LRSP mode for chip communication and long range transmission. So far the selective mode excitation as well as mode convertor has been experimentally demonstrated by two phase controlled beams or theoretically investigated in order to get flexibility in benefiting from two opposing characteristics [10-12].
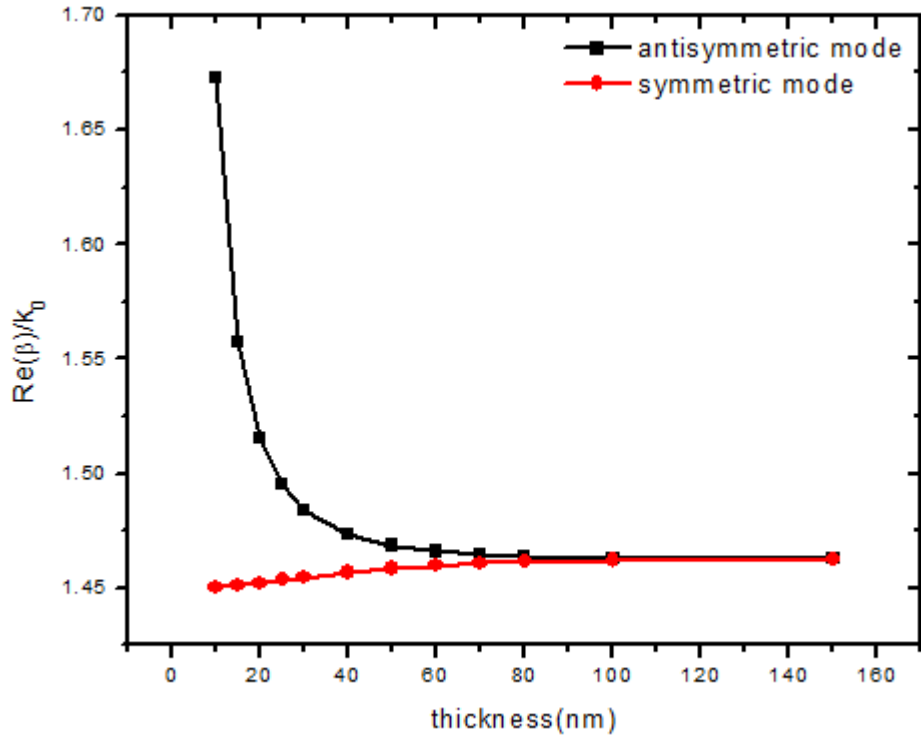
Figure 2.3 Effective index of two propagation modes as a function of thickness at 1.55um
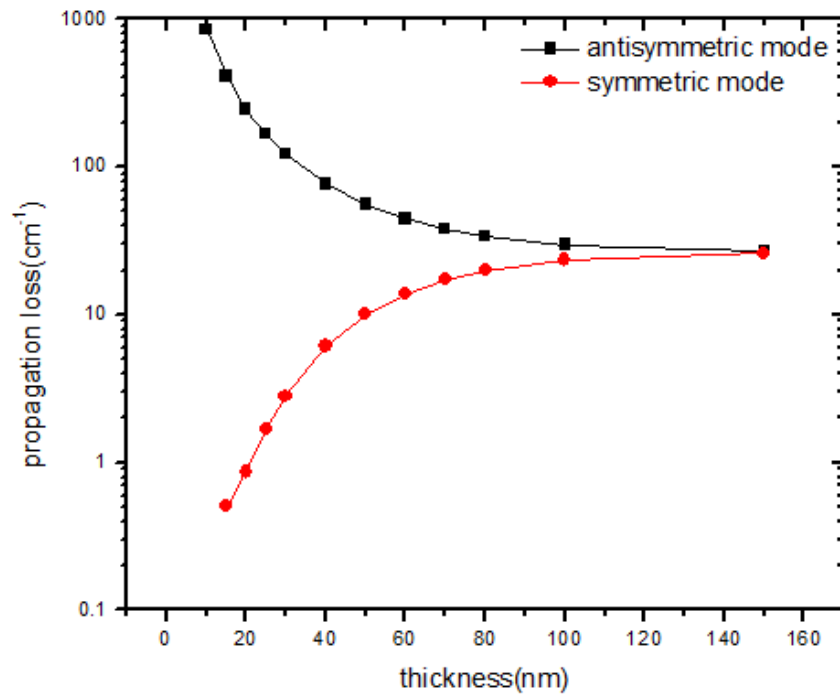
Figure 2.4 Propagation loss of two propagation modes as a function of thickness at 1.55um

In the previous part, we talked about the case for infinite metal stripe embedded in dielectric matrix, next we will discuss finite width case of IMI waveguide. For simplicity, a silver nanowire waveguide, which can be viewed as an IMI waveguide along any direction, is analyzed in the simulation. The structure consists of a silver nanowire embedded in the silicon dioxide with its cross-section view given in Fig2.5(a) .The propagation direction is again perpendicular to the paper. Unlike the modes supported by infinite metal stripe, modes here are not purely TM modes and have all six field due to finite width[12], so we term these modes SRSP-like and LRSP-like modes with electric field distribution given in Fig2.5(b) and Fig2.5(c) respectively.
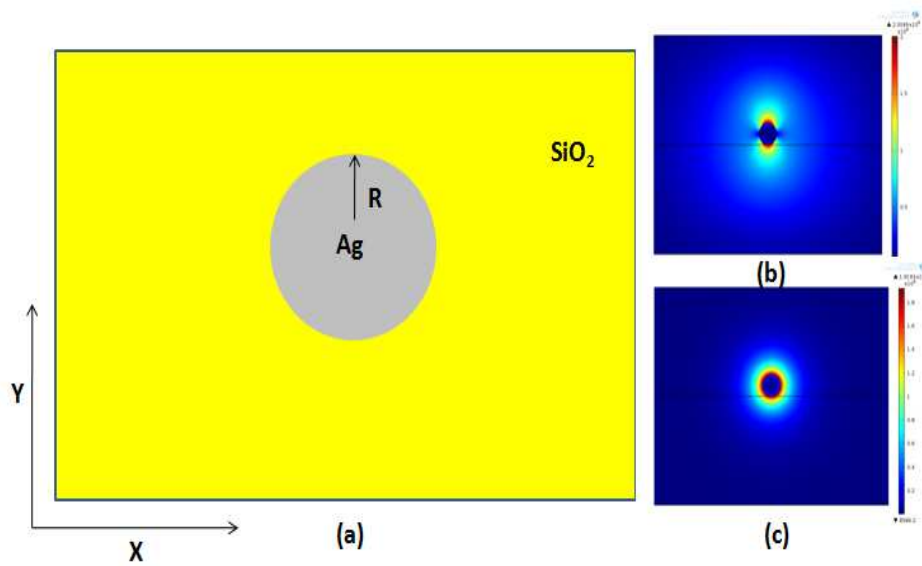
Fig2.5(a) Cross sectional view of silver nanowire embedded in SiO_2 matrix (b)Norm of electric field for SRSP-like mode(c) for LRSP-like mode

The effective refractive index of two modes is shown in Fig2.6 as a function of radius at a vacuum wavelength of 600 nm. Similar to the case with infinite width, the upper branch, which stands for SRSP, goes infinitely with the decreasing radius while the lower branch is decreasing slowly. However, one major difference is that there is a cut off for LRSP-like mode in silver

nanowire waveguide, which is not observable in infinite metal stripe for the same mode. This feature due to the finite width of real structure can be reflected clearly in the plot of propagation loss for each mode given in Fig2.7.As can be seen from figure, the propagation loss of LRSP decreases first then goes up at a turning point with decreasing radius, implying that the guided mode becomes a leaky one. Actually, if you check the effective refractive index in Fig2.5, the value of LRSP modes for radii smaller than 40 nm is below 1.45 (permittivity of SiO_2), proving that this kind of mode has a radius cutoff of 40nm at vacuum wavelength of 600nm.This advantage can be taken to achieve one single mode operation on the silver nanowire by properly designing a smaller radius of nanowire than that of cutoff at a given wavelength. Only SPSP-like mode exists under that condition. In addition, to excite different modes on nanowire in practice, different schemes should be adopted. For SRSP-like mode, the incident polarization should be vertical to nanowire axis while polarization parallel to axis is required to excite LPSP-like one.
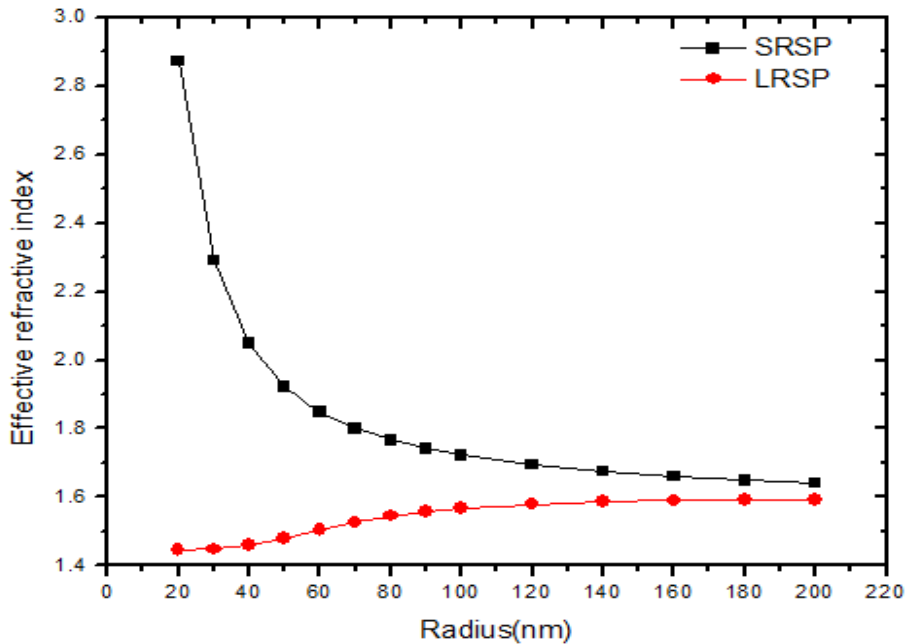
Fig2.6 Effective refractive index of two kinds of modes as a function of radius at600nm
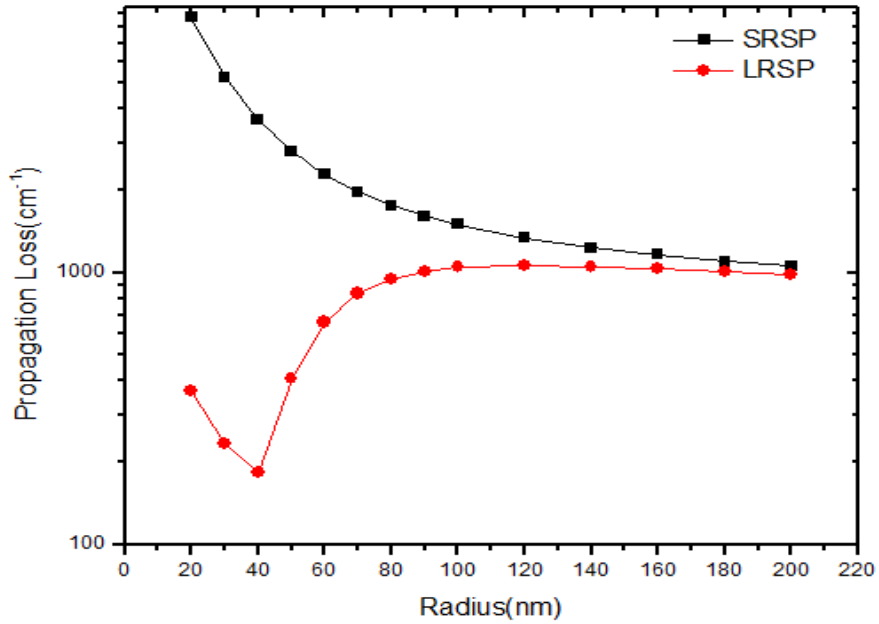
Fig2.7 Propagation loss for SRSP and LRSP with respect of radius at wavelength of 600nm

To further explore substrate effect on the propagating modes, silver nanowire on the substrate (embedded in an asymmetric dielectric) is studied with cross section view given in Fig2.8(a).Unlike the nanowire without substrate, It can only support SRSP-like mode (asymmetric) due to break of symmetry with respect to Y=0 cutline in the Fig2.7.The field distribution of a guiding SRSP-like mode is shown in Fig2.8(b) with a saturated color bar used. We can observe much more field concentrates in the SiO_2 side than that in air side due to the substrate drawing effect. However, leaking issue might become severe at a certain wavelength range where the effective refractive index is smaller than the permittivity of SiO_2 and propagation loss dramatically increases. Fig2.8(c) gives a field distribution of a leaking SRSP-like mode and effective index with respect to wavelength for radius of 45nm and 50nm is provided as well in Fig2.9. As can be seen from the figure, the cutoff wavelength for radius of 45nm and 50nm is 921nm and 826nm, respectively, which means that the operation wavelength

cannot exceed 921nm and 826nm for radius of 45nm and 50nm to achieve mode guiding. Thus, the introduction of a different substrate to supersubstrate imposes a new cutoff condition on the radius of nanowire and operation wavelength for SRSP-like mode.
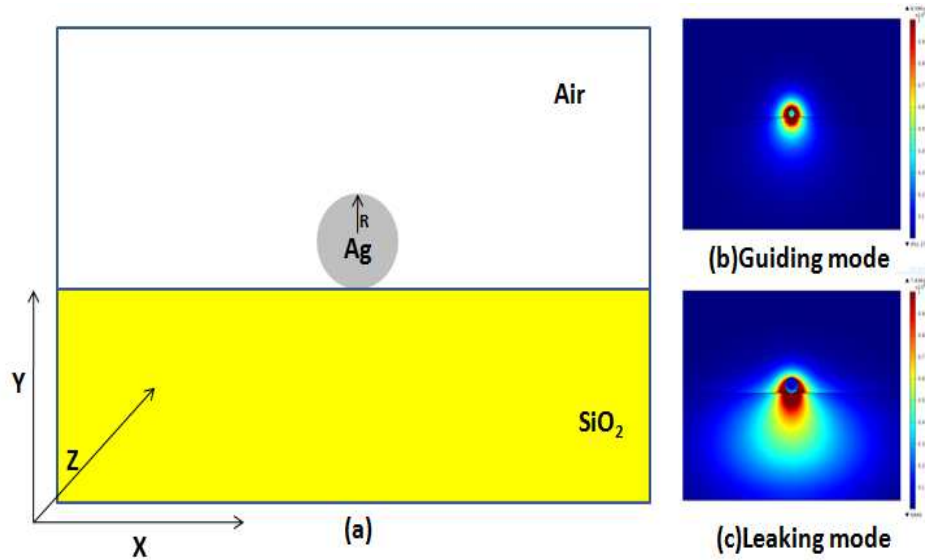
Fig2.8 Cross sectional view of silver nanowire on SiO_2 substrate (b) Norm of electric field for SRSP-like guiding mode(c) for leaking mode
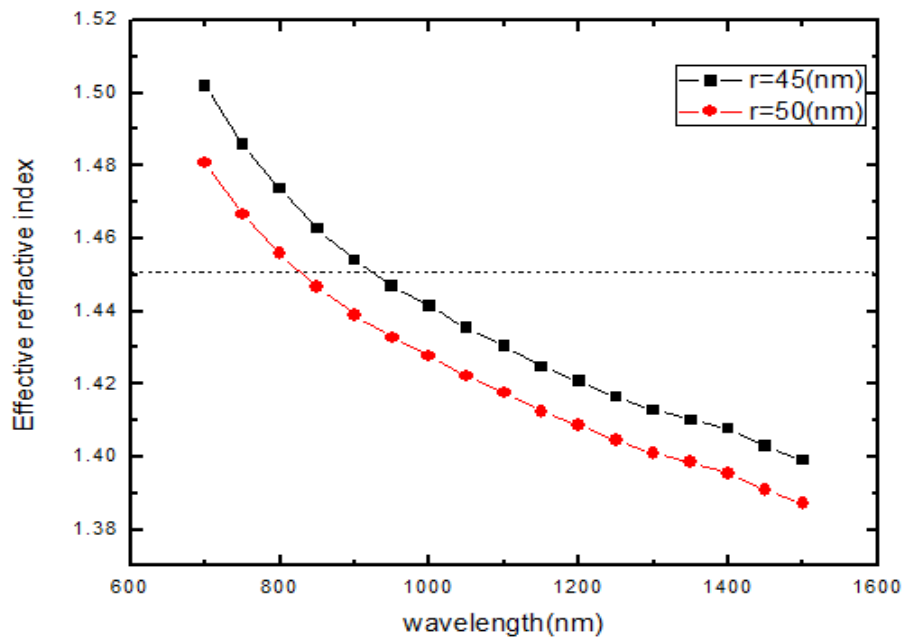
Fig2.9 Effective refractive index of SRSP-like mode versus wavelength for different nanowires

2.2 Metal-Semiconductor-Metal waveguide

In the last section, we talked about one prototype IMI waveguide and particularly one appealing application in nanowire form. For this section, another important plasmonic waveguide, namely Metal-Semiconductor-Metal waveguide (MSM) will be discussed in terms of modes characteristics. We have given an introduction to surface plasmon polariton in 2D MIM structure in the last chapter, showing its unique ability to manipulate light in nanosacle. Hereafter we focus mainly on the propagation characteristics for both symmetric mode and antisymmetric mode in the infinite long waveguide structure. Fig2.10 gives a cross sectional view of MSM structure with propagation direction in Z direction. Semiconductor core GaAs with refractive index 3.59 is used in the simulation.
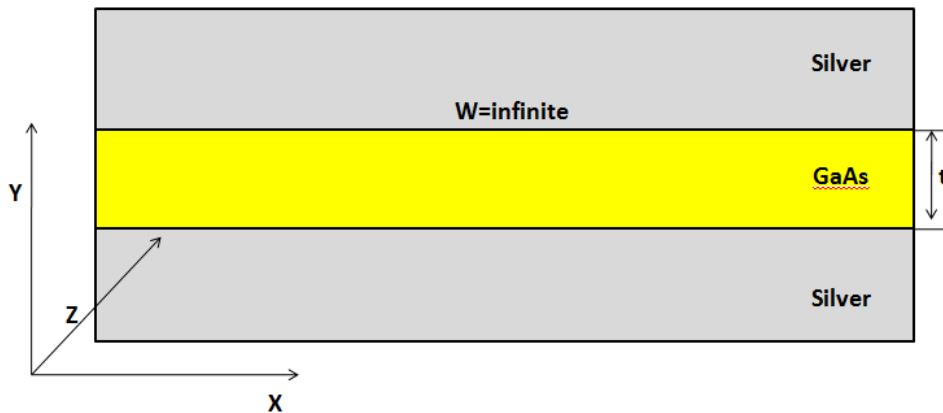
Fig2.10 Cross sectional view of MSM waveguide with infinite width

As the same analogy IMI waveguide has, this structure can be treated as two separately propagating Metal-Semiconductor waveguide as well. With thickness of core layer t is below to certain level, the interaction of vertical surface plasmons occurs which lead to a splitting of single mode in to symmetric case and antisymmetic case. Here the thickness is fixed at100nm where the interaction is occurring .The field distribution of each mode at vacuum wavelength 650nm is given in Fig2.11. As can be seen from the figure, the electric field component Ex

(perpendicular to the metal interface) resembles an even function or odd function for symmetric mode and antisymmetric mode respectively [13].
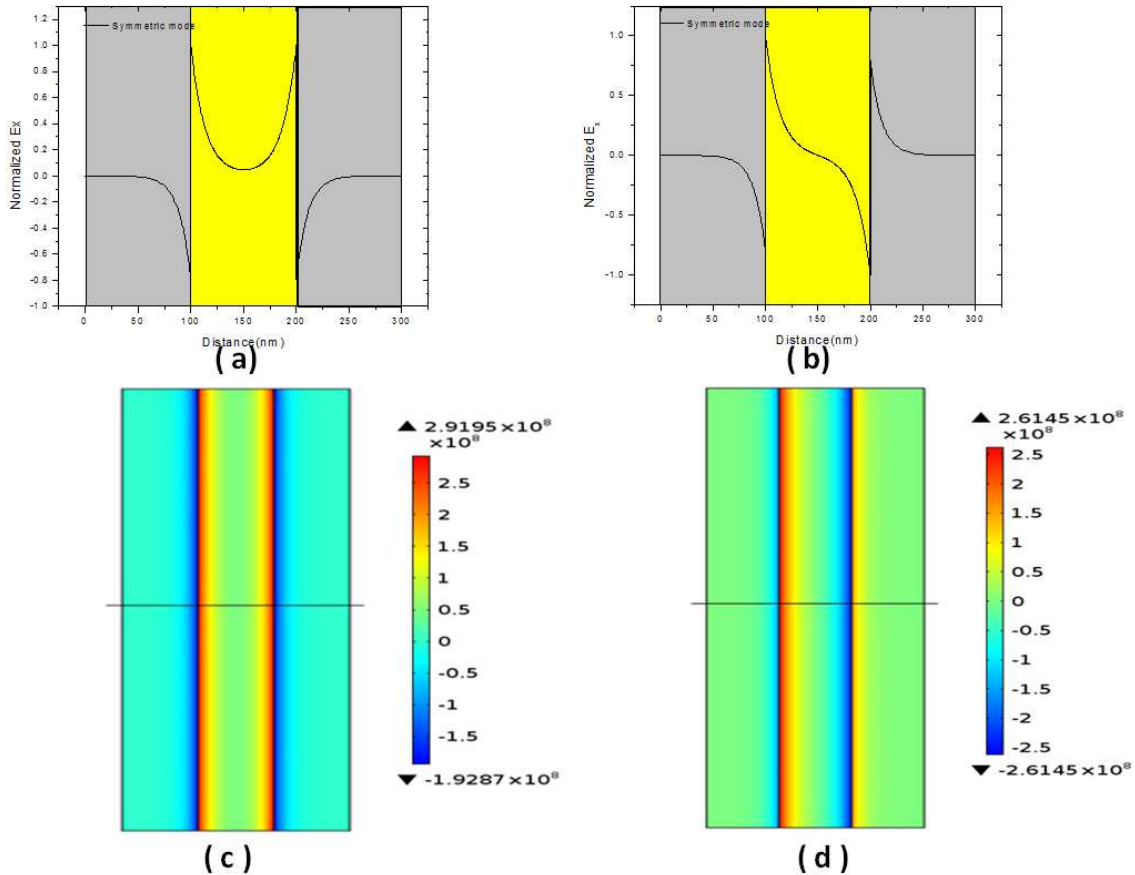
Fig2.11 Field profile Ex for (c) antisymmetric mode and for (d) symmetric mode at 650nm with distribution along the indicated black line given in (a) and (b)

The effective refractive index as a function of wavelength at a fixed thickness 100nm is shown in Fig2.12. As can be seen from the figure, two curves asymptotically approach a certain value as wavelength is close to metal plasmon resonance, which is rightly a characteristics owned by surface plasmon waves. Another feature is antisymmetric mode has a cutoff at a low frequency side as effective refractive index decreases quickly with increasing wavelength. In terms of propagation loss, both modes have a dramatic increase of it when wavelength approaches resonance as can be seen in Fig2.13. This can be attributed to much more energy dissipation in to the metal at high photon energies, which is implied as well from increasing

effective index. It should be noted here that the propagation loss for symmetric mode is decreasing consistently until to a certain level with the increasing wavelength while the loss for antisymmetric mode would decrease first then increase after that due to cut off of the mode as can be seen in the inset of the figure plotted in the logarithm scale.
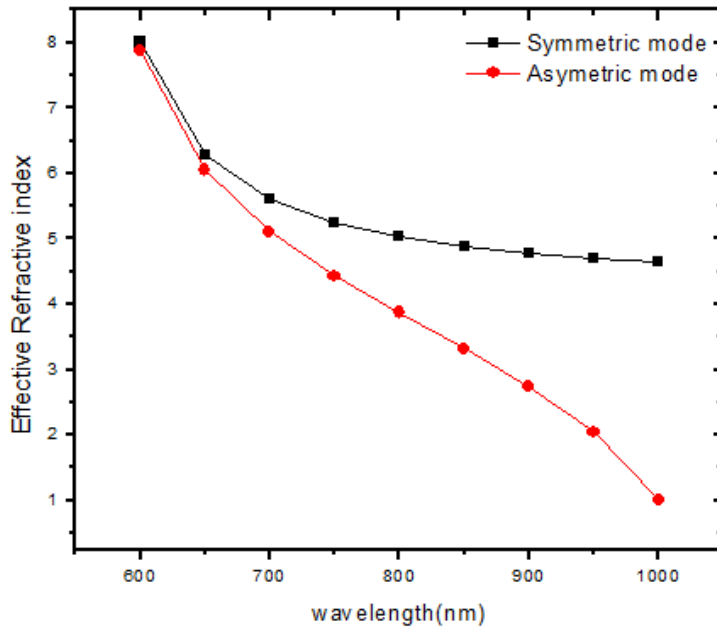
Fig2.12 Effective refractive index as function of wavelength for t=100nm
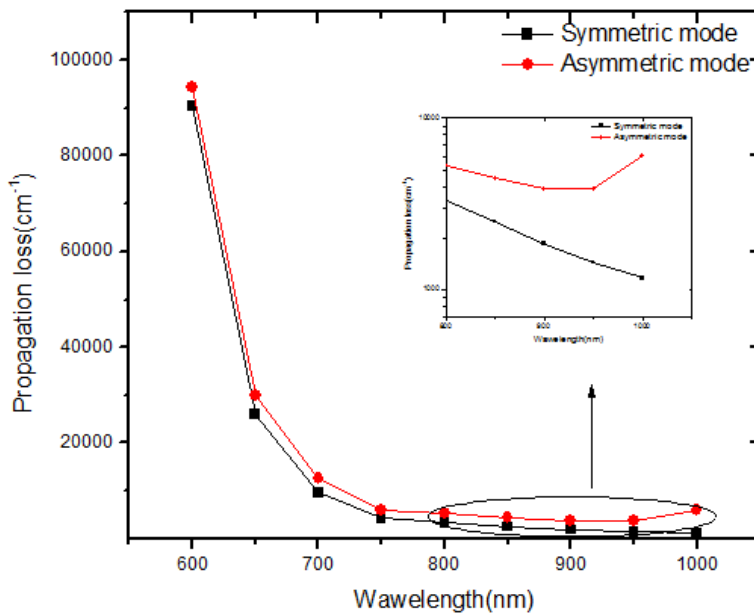
Fig2.13 Propagation loss versus wavelength for t=100nm

2.3 Metal-Insulator-Semiconductor-Insulator-Metal waveguide

Similar to MSM waveguide, Metal-Insulator-Semiconductor-Insulator-Metal waveguide is a multilayer structure with insulators in between at both sides as name indicated. The incorporation of insulator layer is either used for preventing short circuit while electrical pumping [14,15] or acting as a buffer layer for optical modes [16,17].The cross sectional view of MISIM waveguide is given in Fig2.14 with propagation in Z direction. Here the insulation layer is Al_2O_3 (n=1.7) while other parts stay unchanged compared to MSM waveguide. Actually we can view it as an inhomogeneous MSM waveguide which also supports two kinds of modes-antisymmetric mode and symmetric mode. Since inhomogeneous MSM waveguide should have same modal characteristics as that of homogenous one except that the field energy is enhanced at the insulator region due to electric field continuity, we only choose symmetric mode to analyze as a representative of plasmonic mode.
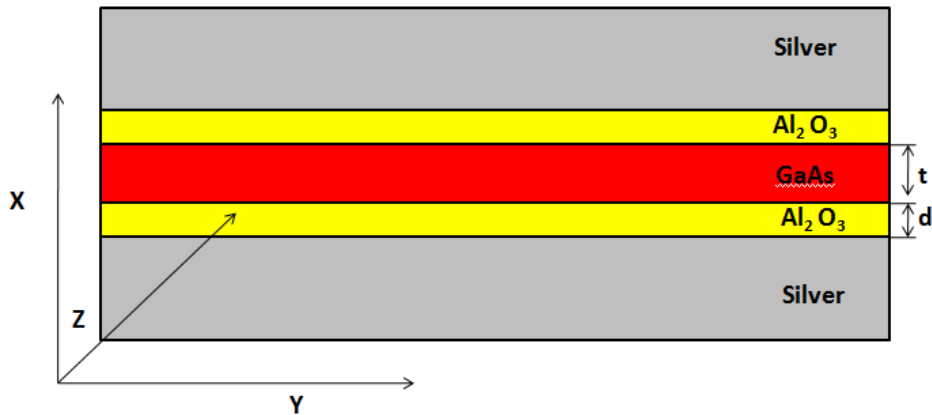
Fig2.14 Cross sectional view of MISIM waveguide

In the simulation, the thickness of insulation layer is fixed at 20nm while that of semiconductor core layer is varied. Fig2.15 gives the field distribution of the modes propagating in the waveguide with t=300nm. TM-like mode which has most of its field across the insulator layer is actually a distortion of symmetric plasmonic mode in the homogenous MSM waveguide due to introduction of low permittivity layer. This mode has a dominating field component

29

perpendicular to the metal surface(X direction) which is a nature for surface plasmon waves. The other mode with most of energy confined in the semiconductor core has dominating field along the Y direction and little electric field component in Z direction. So we call this mode TE-like mode.
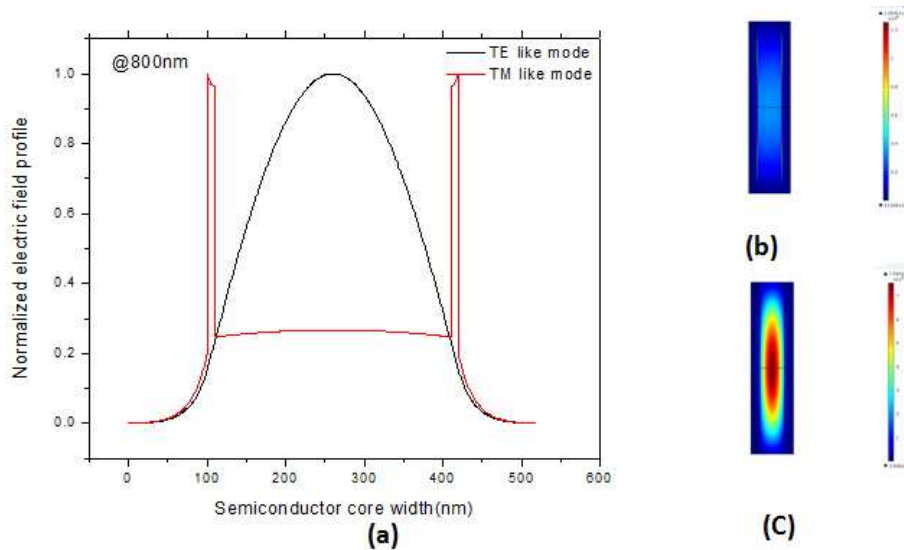
Fig2.15 (a) Norm of electric field distribution along the black line indicated at (b) TM-like mode and (c) TE-like mode

The effective refractive index and propagation loss for each mode as a function of semiconductor core width at vacuum wavelength 800nm are shown in Fig2.16.The red square represents TE- like mode while black cube stands for TM-like mode with effective index and propagation loss indicated in the left and right axis separately. As can be seen from the figure, the TE mode sees a cut off around 100nm (roughly diffraction limit) as indicated by dramatically increased propagation loss and massively decreased effective index. For TM-like mode, the effective index decreases flatly with the decreasing of core width showing a possibility of indefinite shrinking of semiconductor width in theory. However, the propagation loss is increased significantly with the decrease of width, meaning much larger gain is required to achieve lossless propagation at the smaller width far beyond the diffraction limit.
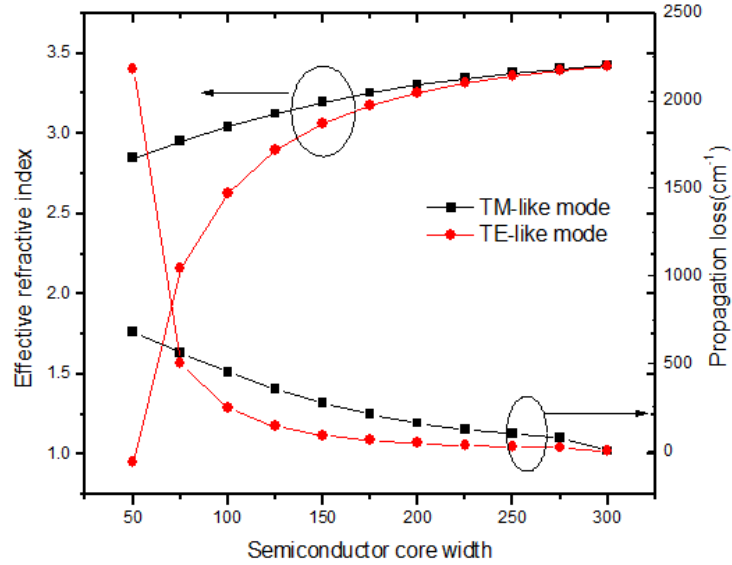
Fig2.16 Effective refractive index and propagation loss for TM-like mode and TE-like mode versus semiconductor core with at 800nm

2.4 Summary

Plasmonic waveguides of different configurations and geometries are investigated in this chapter. Modal characteristic for each waveguide is given. For IMI waveguide, there are two propagating modes due to coupling of two single surface plasmons , which results in different phases of charge oscillations. One is antisymmetric mode (SRSP) with strong confinement capability and relatively low propagation length while the other one is symmetric mode (LPSP) which has poor confinement capability and long propagation loss. This kind of mode splitting phenomena is observed as well in nanowire waveguide and MSM waveguide. In contrast to IMI waveguide which has no cutoff for both modes, nanowire waveguide has radius cutoff for symmetric mode arising from finite width and a wavelength cutoff for only-propagating antisymmetric mode in the case with substrate. High energy mode in MSM waveguide shows frequency cutoff as well. Lastly, a comparison of TM-like and TE-like mode in MISIM waveguide shows potential of plasmonic mode in shrinking the width.

31

CHAPTER 3

PLASMONIC NANOLASER

3.1 Metal-Semiconductor-Metal nanolaser cavity

Previously we talked about different plasmonic waveguides using surface plasmon polariton which affords a unique ability to confine light in subwavelength scale. In this chapter, we focus on this feature employed on the nanolaser. The miniaturization of laser has been an ever-increasing demand for community since there is still a size mismatch between electronic device and photonic device .In order to combine these two in one chip with high dense integration, one must shrink photonic device such as lasers to the size comparable to electronic transistors for on-chip communication.

Recently metal has been playing an important role to achieve the subwavelength confinement to further shrink laser cavity. Generally there are two different approaches with the same metal cladding. One is use metal-optic cavity to confine optical mode as demonstrated in [18,19].In this case ,the metal serves as only an efficient reflector as it always does in microwave community. The mode can be confined well with reduced radiation loss and modal volume. The other case is to utilize truly surface plasmon to confine light as demonstrated in [20-23] .Using of plasmonic mode can break diffraction limit and make an ultra-small laser in three dimensions. However, it would subject to severe metal loss due to strong interaction between electrons and photons. Normally the cavity of optical mode requires larger dimension than plasmonic mode while the plasmonic mode has larger loss than optical mode.

To examine quantitatively the cavity performance of two modes such as quality factor, modal volume and threshold gain, we investigate a prototype metal-semiconductor-metal cavity shown in Fig3.1 which can support plasmonic mode and optic mode simultaneously in the

infrared regime. Similar to metal-semiconductor-metal waveguide, the cavity consists of semiconductor disk sandwiched by two metal disks. The semiconductor disk is used to provide gain and metal disks serve as either a reflective mirror or source for electrons coupled in to plasmonic mode to achieve confinement.
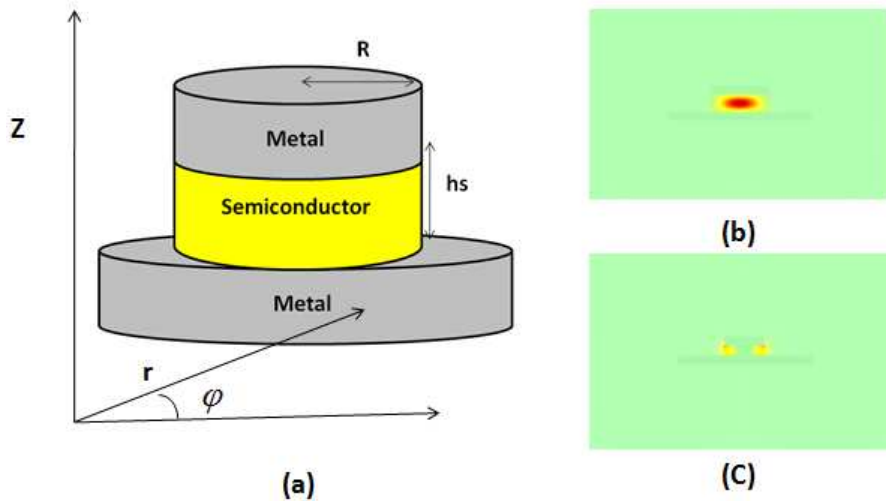
Fig3.1 (a) Schematic diagram of Metal-Semiconductor-Metal nanolaser cavity (b) optical mode(c) plasmonic mode

Fig 3.1(b) and Fig3.1(c) give intensity distribution of examples of optical mode and plasmonic mode respectively. Generally there are three ways to distinguish them. (1) The field intensity maximum of plasmonic mode lies at the boundary of metal and dielectric while that of optic mode occurs far away from metal. (2)Plasmonic mode can break diffraction limit to a deep subwavelength confinement while optic modes can't.(3)Plasmonic mode has a dominant field component vertical to metal surface while optic mode has no preference direction though it has dominant polarization. Section 3.2 and 3.3 will give details about optical mode and plasmonic mode separately. After that a comparison between two modes in terms of cavity performance including QED effect and lasing threshold will be presented in section3.4.

3.2 optical modes

The optical modes supported in the above structure can be obtained by assuming metal as a perfect electrical conductor(PEC) and semiconductor side wall as a perfect magnetic conductor(PMC).This approximation which is excellent in microwave regime can also be adopted here in near-infrared region to capture profiles and symmetries of the cavity modes since no surface plasmons exist in this region for optical mode[24].Thus, in terms of eigenmodes function, we can borrow an idea from micro-patch antenna which is the bigger version of above structure. The notation TE_{mnp} and TM_{mnp} is used to specify particular mode for this cavity, where m,n,p represent azimuthal, radial and axial modal numbers. The fundamental TM mode and TE mode are TM_{110} and TE_{011} mode respectively .However, TM_{110} mode is the mode of choice of circular micropatch antennas at RF/microwave frequencies [25] as an efficient radiator and not suitable for laser application, here we refer TM_{111} and TE_{011} as the most fundamental TM mode and TE mode with their field profiles given in cylindrical coordinates below:

$$TM_{111}:$$

$$E_z(r,\phi,z) = -E_0 J_1(k_{r,TM_{111}} r)\cos(\frac{\pi}{h}z)\sin(\phi)$$

$$E_r(r,\phi,z) = -E_0 \frac{\pi}{h\,k_{r,TM_{111}}} J_1'(k_{r,TM_{111}} r)\sin(\frac{\pi}{h}z)\sin(\phi)$$

$$E_\phi(r,\phi,z) = -E_0 \frac{\pi}{h\,k_{r,TM_{111}}} \frac{J_m(k_{r,TM_{111}} r)}{k_{r,TM_{111}} r}\sin(\frac{\pi}{h}z)\cos(\phi)$$

$$TE_{011}:$$

$$H_z(r,\phi,z) = -H_0 k_{r,TE_{011}}^2 J_0(k_{r,TE_{011}} r)\cos(\frac{\pi}{h}z)$$

$$H_r(r,\phi,z) = H_0 \frac{\pi\,k_{r,TE_{011}}}{h} J_0'(k_{r,TE_{011}} r)\cos(\frac{\pi}{h}z)$$

$$E_\phi(r,\phi,z) = iH_0 \omega\mu\, k_{r,TE_{011}} J_0'(k_{r,TE_{011}} r)\sin(\frac{\pi}{h}z)$$

$$H_\phi(r,\phi,z) = E_z(r,\phi,z) = E_r(r,\phi,z) = 0$$

where $k_r^2 = (\omega_{mnp}/c)^2 \varepsilon - (\pi/h)^2$, h is cavity height ,$\omega_{mnp}$ is cavity resonance frequency and ε is the permittivity of semiconductor medium. FDTD Simulation is performed by MIT made software MEEP to find fundament optical modes. Mode patterns of TE_{011} and TM_{111} are given in

Fig3.2. Each component of electric field which is not shown here also agrees well with analytic equations. One thing should be noted here different source polarizations are required to excite different modes due to match of field distribution.

(a) TM$_{111}$ **(b) TE$_{011}$**

Fig3.2 Field intensity $\left|E\right|^{2}$ for (a) TM$_{111}$ mode and (b) TE$_{011}$mode

Although no surface plasmon is involved in this optical mode, there is still interaction between metal and electromagnetic mode which confine light into a small modal volume with a decent Q. Simulation shows for a cavity with height 230 nm and radius 250nm,TM$_{111}$ has a modal volume $0.5(\frac{\lambda}{2n})^{3}$ and Q is 250 while TE$_{011}$ has a modal volume of $2.9(\frac{\lambda}{2n})^{3}$ with Q about 143.Of them TM$_{111}$ is considered as the most potential mode in lasing application since it represents the most fundamental moderate Q mode with a subwavelength modal volume .In the section 3.4, we will use this mode as a representative of optical mode to make a full comparison with plasmonic mode which is supported in this structure as well .

3.3 Plasmonic mode

We discussed in the last section about optical modes which are diffraction limited. In order to further shrink the device far beyond the limit, surface plasmon modes must be employed to achieve deep-subwavelength confinement owing to its unique property in manipulating light at nanoscale. In this metal-semiconductor-metal laser cavity, surface plasmons can be formed in the semiconductor region like that propagating in the MSM waveguide we talked earlier. The coupling between two metal-semiconductor interface leads to the splitting of mode in to two (symmetric and antisymmetric). Antisymmetric mode has a wavelength cutoff and difficult to excite due to metal skin effect, thus the focus of plasmonic mode is on symmetric one. The dispersion relationship for symmetric mode is given in the following:

$$\varepsilon_m k_d \tanh(k_d t / 2) = -\varepsilon_d k_m$$

where $k_d^2 = k_{spp}^2 - \varepsilon_m \dfrac{\omega^2}{c^2}$, $k_m^2 = k_{spp}^2 - \varepsilon_d \dfrac{\omega^2}{c^2}$ .Simulation did in the section1.3 shows MSM plasmonic mode has much larger wavevector or momentum as wavelength approaches resonance wavelength or the thickness of semiconductor is become thin. The high momentum enables more possibility of the mode to undergo internal reflection around disk circumference with necessary feedback forming whispering gallery (WG) plasmonic mode. The resonance condition of whispering gallery mode is given:

$$k_{spp} R = m (m = 1, 2, 3, ...)$$

where k_{spp} is the wavevector of plasmonic mode, R is the radius of disk, and m is an integer. It's clear to see here that since k_{spp} increases with the decrease of thickness in vertical direction, R in the planar direction should be decrease as well to maintain at the same wavelength. This provides an opportunity to achieve full three-dimensional subwavelength confinement as discussed in [26, 27].we will present this point in details later with simulation results. The WG mode profile with

36

an azimuthal number m of 4 is shown in Fig3.3. Here the 2D axial symmetry simulation is used to exploit cylinder symmetry. As can be seen from the Fig3.3, the field is confined tightly in the vertical direction between metals. Linear dependence on radius in contrast to saturating behavior of TM_{111} mode in Fig3.4 proves it is a WG mode.

(a) $|E|^2$ profile for m=4,radial order 1

(b) $|E|^2$ profile for m=4,radial order 2

(c) E_z profile for m=4,radial order 1

(d) E_z profile for m=4,radial order 2

Fig3.3 Field intensity and z component of electric field for WG plasmonic mode (m=4)
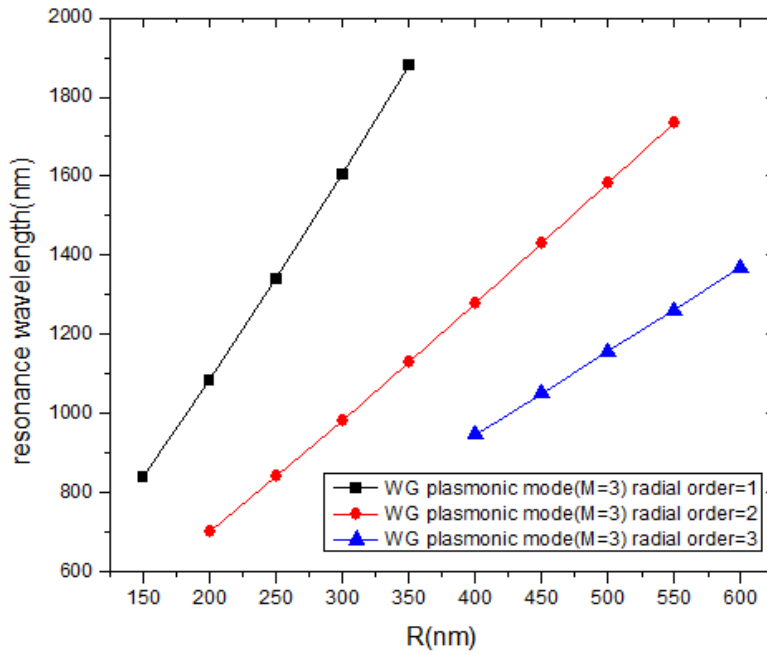

Fig3.4 Resonance wavelength versus R for WG plasmonic mode (m=4)

3.4 comparative study of optical mode versus WG plasmonic mode

In the last two sections, we talked about optical mode and plasmonic mode in the metal-semiconductor-metal disk cavity respectively. While it's been intensively investigated in the field of plasmonic waveguide utilizing surface plasmon to achieve both subwavelength confinement and long transmission, the advantages or drawbacks of surface plasmon lazing should be examined in details as well. Thus, this section is about a comparison of two distinctively different modes with metal confinement in common in terms of cavity performance such as Q ,V related to the light-matter interaction and threshold gain which is a key parameter of lazing characteristics.

For optical modes, we adopt TM_{111} mode as a representative of them since it's the fundamental moderate Q mode with a subwavelength modal volume. For plasmonic modes, only the fundamental modes in radial and vertical directions are discussed as these modes have high Q and small modal volume than high order modes in those directions. Azimuthal modal number of 2 is investigated first as azimuthal number of 1 corresponds to dipole resonance with serious radiation loss, which degrades Q massively.

In order to give a fair comparison, telecommunication wavelength at 1.55um is chosen as a guideline for cavity design. The resonance wavelength dependence on the radius with different height hs for different modes is given in Fig3.5 and Fig3.6 respectively. As we discussed in the section 3.3, unique characteristics of plasmonic wave can enable full-3D mode confinement with size reduction in all three dimensions. The resonance wavelength for TM_{111} mode increases with the increase of both cavity radius and cavity height, which is a normal behavior for conventional semiconductor laser. However, for plasmonic mode, the resonance wavelength increases with radius but decreases with height meaning that it can be confined in a 3D

38

simultaneously shrinking cavity while maintaining at the same wavelength. This point can be further illustrated by insets in each figure giving cavity dimensions corresponding to wavelength of 1550nm.
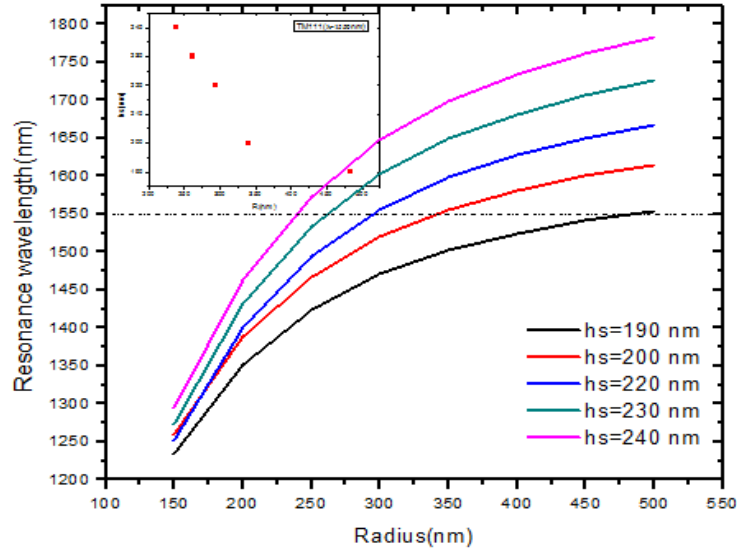
Fig3.5 Resonance wavelength versus radius at different height for TM_{111}mode.Inset shows cavity dimension(R,hs) at 1550nm
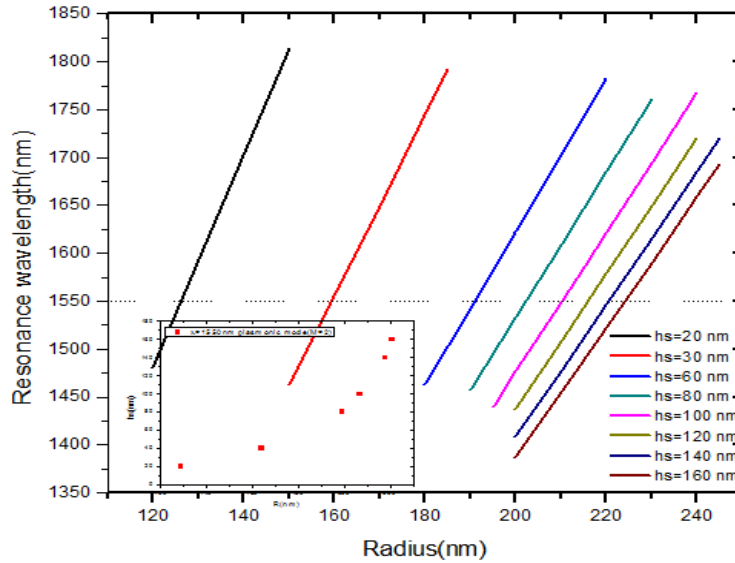

Fig3.6 Resonance wavelength versus radius at different height for WG plasmonic mode (m=2).Inset shows cavity dimension(R,hs) at 1550nm

In order to investigate light matter interaction at fixed wavelength 1550nm for two different modes, modal volume and purcell factor are calculated in Fig3.7 and Fig3.8 as a

function of physical volume which is obtained from structure parameters of the red spot in the insets of Fig3.5 and Fig3.6 . Here the modal volume is calculated as [28]:

$$V_{eff} = \frac{\int \varepsilon(x, y, z)|E(x, y, z)|^2 dxdydz}{\max\{\varepsilon(x, y, z)|E(x, y, z)|^2\}}$$

and Purcell factor is defined by[28]:

$$F_p = \frac{3}{4\pi^2}(\frac{\lambda}{n})^3(\frac{Q}{V_{eff}})$$

where λ means resonance wavelength in vacuum and n is the refractive index of semiconductor medium. As can be seen from the figures, firstly, plasmonic mode indicated by red squares enables further shrink of device volume which is an advantage obtained from surface plasmon. Then, as the semiconductor physical volume decreases, the purcell factor for plasmonic mode increases dramatically and modal volume decreases massively meaning highly enhanced light matter interaction occurring inside the cavity which is desirable for a laser application. In contrast to plasmonic mode, optical TM_{111} mode has much less potential to achieve both high Purcell factor and small modal volume as can be shown by black spots and implied by crowded spacing of them while decreasing the physical volume. Here the Purcell factor of 6238 in a modal volume of 0.001 $(\frac{\lambda}{2n})^3$ for plasmonic mode at 1550nm at room temperature can be achieved in a cavity with height of 20nm and radius of 129 nm, which is the highest value reported so far according to our knowledge. It's important to note that the thickness of semiconductor can be indefinitely small in theory to exploit cavity QED effect of plasmonic mode further and here thsmallest thickness is only set to 20nm due to 2nm of spatial resolution used in FDTD simulation.
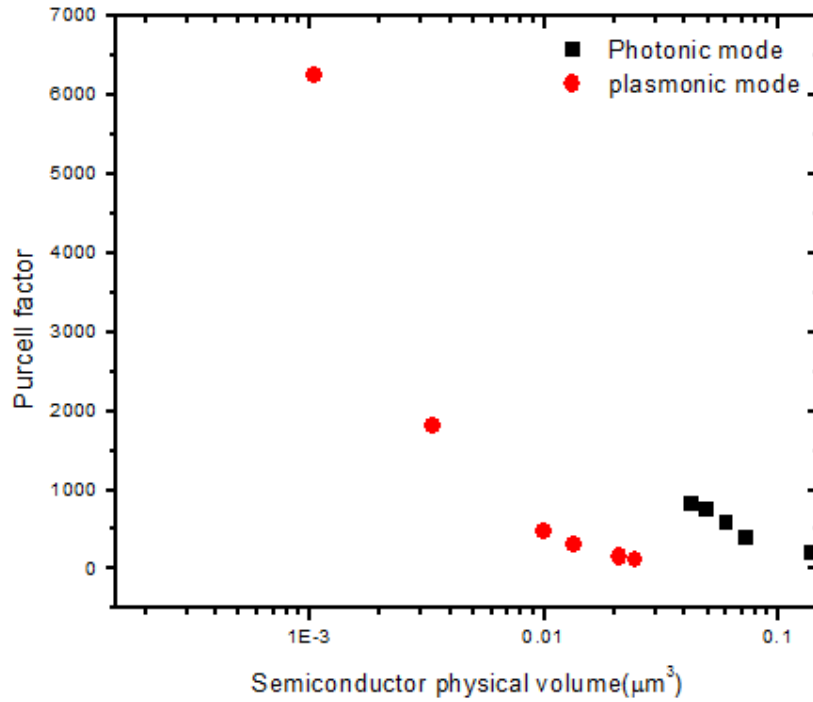
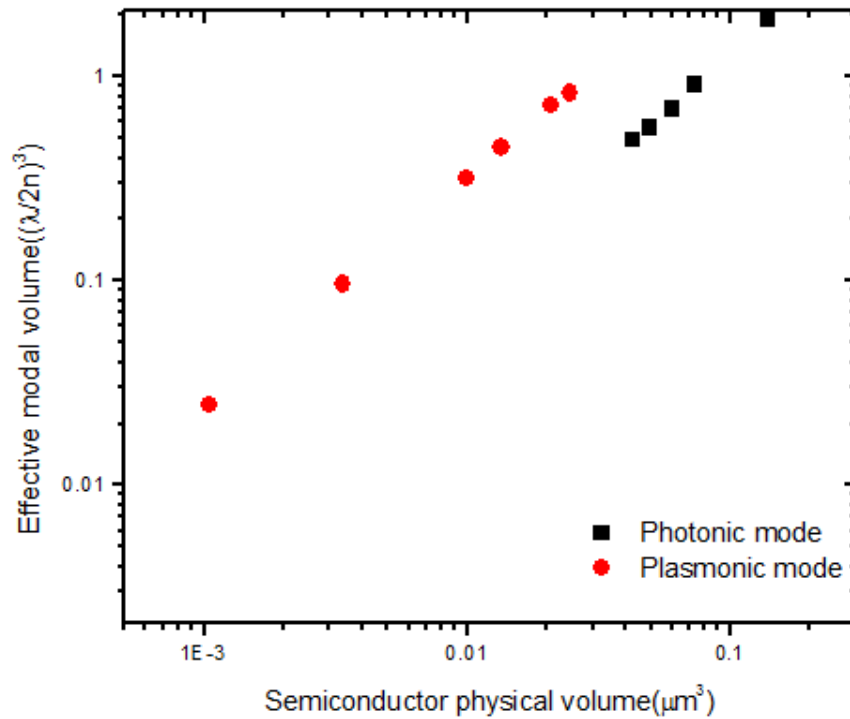Fig3.7 Purcell factor as a function of semiconductor physical volume for modes at 1550nm

Fig3.8 Effective modal volume as a function of semiconductor physical volume for modes at 1550nm

41

In order to examine whether such cavity modes can achieve lasing at room temperature, the gain material threshold gains as a function of physical volume for both modes at 1550nm are given in Fig3.9(a) calculated by[29]:

$$g_{th} = \frac{2\pi n_g}{Q\Gamma_E\lambda}$$

where n_g means group material index, Γ_E is energy confinement in semiconductor gain medium , λ is vacuum wavelength .As can be seen from the figure, the threshold gain for TM$_{111}$ optical mode indicated by black square is below that of plasmonic mode represented by red spot, which is expected since truly plasmonic mode involves stronger photon-electron interaction than optical mode leading to large loss and small threshold gain. Interestingly, As the physical volume decreases, the threshold gain of plasmonic mode decreases first then increases leading to a minimal threshold gain of 2300 cm^{-1} which is achievable at room temperature by using InGaAsP/InP quantum well as a gain region with electrical pumping[30].This feature is attributed to the interplay of radiation loss and metal loss in the plasmonic system as reflected in Fig3.9(b) which gives Q dependence on semiconductor gap thickness .The optical Q and absorption Q of plasmonic mode which are inversely related to optical loss and metal loss are separated from the total Q in the figure .One can observe that optical Q increases dramatically with decreasing gap thickness. This can be explained by high effective index induced by plasmonic mode to prevent radiation loss. In contrast to optical Q, absorption Q decreases as gap become thin, which can be understood by more electrical field overlap with metal leading to a large absorption loss. Total Q curve approaches absorption Q curve at the thin gap part which means metal loss limits the total loss in this region where optical loss are extremely small indicated by much high optical Q. As the gap becomes thick, the optical loss dominates as total

Q curve approaches decreasing curve of optical Q .The combination of these two lead to a maximum of total Q and finally a minimum of threshold gain at a thickness of 40nm.One thing should be noted that although this minimum threshold gain is nearly three times as large as that of TM_{111} mode, high Purcell factor of 1836 and small modal volume of 0.09 $(\frac{\lambda}{2n})^3$ are achieved far beyond the optical mode can attain in a cavity with radius of 164nm and semiconductor height(gap) of 40nm.
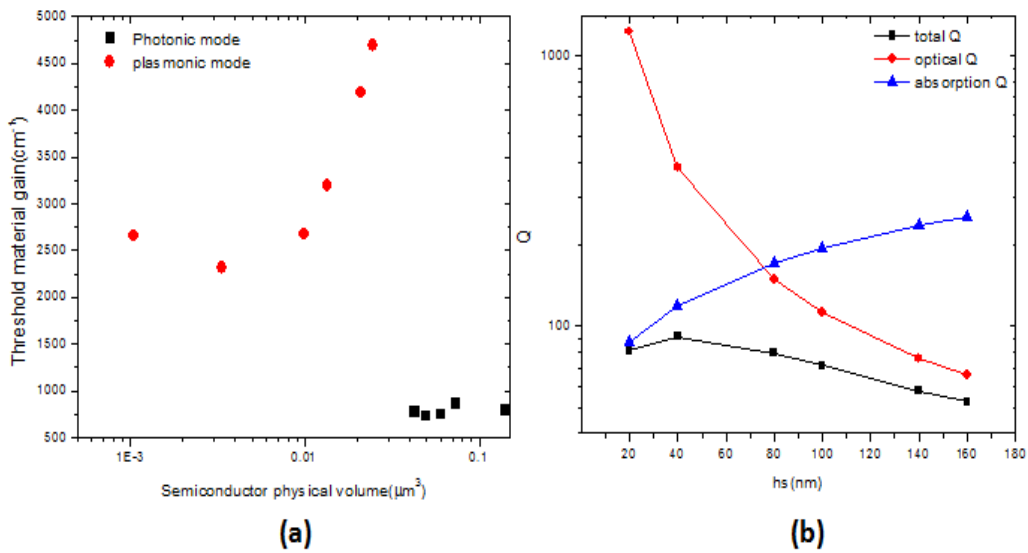

Fig3.9(a) Threshold gain with respect to semiconductor physical volume for plasmonic mode (red) and optical mode (black). (b) Different quality factors versus semiconductor height.
However, although this minimum threshold gain is achievable at room temperature, high carrier density in the quantum well under a high pumping level is required. Another concern is the thermal management associated with high pumping particularly in a densely packed array of such devices. Thus, It's extremely important to reduce the threshold gain of plasmonic mode further for a reasonable compensation in practice .One method is to operate it at a cryogenic temperature which would decrease lasing threshold a lot but would prevent wide application in normal condition. The other method is to use a larger radius device to support high azimuthal number mode with resonance wavelength staying the same. This high azimuthal number mode in

a large device can mitigate radiation loss and even make the total Q approach its metal loss limit.

The threshold gain for plasmonic mode with azimuthal number of 5 is shown in Fig3.10 with

original data in Fig3.9(a) as a comparison As can be seen from the figure, threshold gains for

high azimuthal number m=5 bridge the gap between low azimuthal one and optical one ,which

makes threshold requirement easy to fulfill in a more compact device(compared to optical

mode).However, one thing should be pointed out that although the gain threshold is reduced in a

still compact device with high azimuthal number mode m=5 ,the QED advantage would not be

taken as well as low azimuthal number one due to increasing modal volume accompanying with

large device.
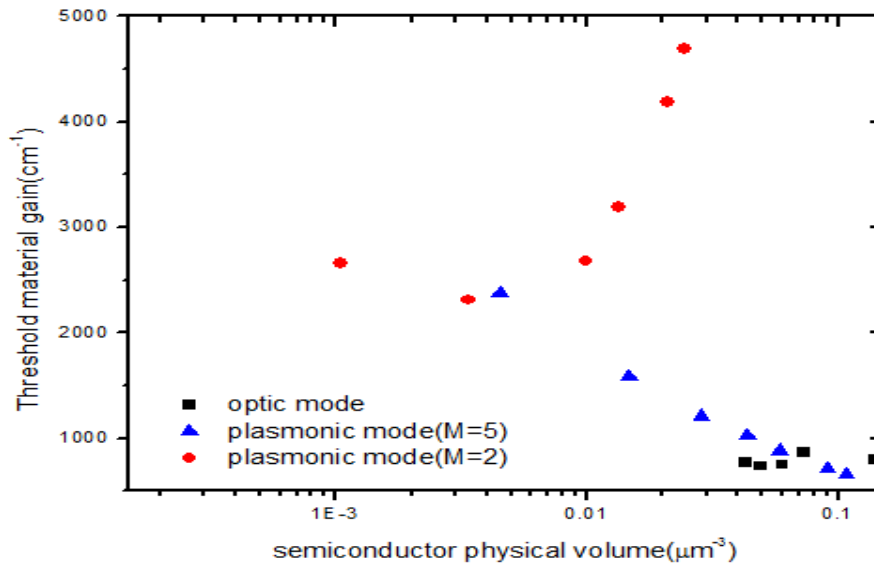
Fig3.10 Threshold gain versus semiconductor physical volume with plasmonic mode (m=5) added

In summary, we have compared surface plasmon mode and optical mode in metal-

semiconductor-metal cavity in terms of cavity performance by FDTD simulation for room

temperature and at the telecommunication wavelength. The results show quantitatively

plasmonic modes in resonator have advantages over optical modes in scalability down to small

size and QED performance due to possibility of breaking the diffraction limit. Surprisingly,

although plasmonic mode have large loss as expected, minimal achievable threshold can be attained for WG plasmonic mode (m=2) by optimizing device parameters at 1.55um due to interplay of metal loss and radiation loss. We further show plasmonic modes with high azimuthal number have smaller threshold gain compared to low azimuthal ones with the same scaling ability.

REFERENCES

[1] G.V. Naik, V.M. Shalaev, A. Boltasseva, "Alternative Plasmonic Materials: Beyond Gold and Silver", Adv. Mater. 25, 3264-3294(2013)

[2]D. B. Li, C. Z. Ning, "All-semiconductor active plasmonic system in mid-infrared wavelengths", Opt. Express 19(15), 14594-14603(2011)

[3] S. L. Chuang, "Physics of Photonic Devices" (2009)

[4]S. Adachi, "Model dielectric constants of GaP, GaAs, GaSb, InP, InAs and InSb," Phys. Rev. B Condens. Matter 35(14), 7454-7463(1987)

[5] S. Law, D .C. Adams, A. M. Taylor, and D. Wasserman, "Mid-infrared designer metals", Opt.Express20(11),12155-12165(2012)

[6] P. Hageman, W. Schaff, J. Janinski, Z. Liliental-Wener, "n-type doping of wurtzite GaN with germanium grown with plasmona-assisted molecular beam epitaxy",J.Cryst.Growth.267,123-128(2004)

[7] H. T. Miyazaki, Y. Kurokawa, "Squeezing visible light waves into a 3-nm-thick and 55-nm-long plasmon cavity", Phys. Rev. Lett, 96, 097401(2006)

[8] F. Kusunoki, T. Yotsuya, J. Takahara, T. Kobayashi, "Propagation properties of guided waves in index-guided two-dimensional optical waveguides", Appl. Phys. Lett. 86(21), 211101(2005)

[9] J. Takahara, F. Kusunoki, "Guiding and nanofocusing of two-dimensional optical beam for nanooptical integrated circuits" IEICE Trans. Electron. E90-C(1),87-94(2007)

[10]K. Yamamoto, K. Kurihara, J. Takahara, A. Otomo, "Effective excitation of superfocusing surface plasmons using phase controlled waveguide modes", Mater.Res.Soc.Symp.Proc. 1182-EE13-05, 55(2009)

[11] M. Miyata and J. Takahara, "Excitation control of long-range surface plasmons by two incident beams", Opt. Express 20(9), 9493-9500(2012)

[12] J. Takahara and M. Miyata, "Mutual mode control of short-and long-range surface plasmons", Opt. Express 21(22), 27402-27410(2013)

[13] S. W. Chang and S. L. Chuang, "Fundamental formulation for plasmonic nanolasers", IEEE J. Quantum Electron. 44(5), 1014-1023(2009)

[14]K. Ding, Z. C. Liu, L. J. Yin, M. T. Hill, M. J. H .Marell, P .J. vanVeldhoven, R. Noetzel, C. Z. Ning, "Room-temperature continuous wave lasing in deep-subwavelength metallic cavities under electrical injection", Phys.Rev.B85, 041301(2012)

[15] K. Ding, Z. C. Liu, L. J. Yin, M. T. Hill, M. J. H. Marell, P. J. vanVeldhoven, R. Noetzel, C. Z. Ning, "Electrical injection continuous wave operation of subwavelength-metallic cavity lasers at 260 K",Appl.Phys.Lett,98,231108(2011)

[16] M. P. Nezhad, A. Simic, O. Bondarenko, B. Slutsky, A. Mizrahi, L. Feng, V. Lomakin, and Y. Fainman, "Room-temperature subwavelength metallo-dielectric lasers", Nat. Photonics4(6), 395–399 (2010)

[17] A. Mizrahi, V. Lomakin, B. A. Slutsky, M. P. Nezhad, L. Feng, Y. Fainman, "Low threshold gain metal coated laser nanoresonators",Opt.Lett.33,1261-1263(2008)

[18] K. Yu, A. Lakhani, and M. C. Wu, "Subwavelength metal-optic semiconductor nanopatch lasers," Opt. Express 18(9), 8790–8799 (2010)

[19] M. T. Hill, Y.-S. Oei, B. Smalbrugge, Y. Zhu, T. de Vries, P. J. van Veldhoven, F. W. M. van Otten, T. J. Eijkemans, J. P. Turkiewicz, H. de Waardt, E. J. Geluk, S.H.Kwon, Y.H. Lee, R. Nötzel, and M. K. Smit, "Lasing in metallic-coated nanocavities," Nat. Photonics1(10), 589–594 (2007).

[20] S. H. Kwon, J. H. Kang, C. Seassal, S. K. Kim, P. Regreny, Y. H. Lee, C. M. Lieber, and H. G. Park, "Subwavelength plasmonic lasing from a semiconductor nanodisk with silver nanopan cavity," Nano Lett.10(9), 3679–3683 (2010)

[21] M. Kuttge, F. J. García de Abajo, and A. Polman, "Ultrasmall mode volume plasmonic nanodisk resonators," Nano Lett. 10(5), 1537–1541 (2010)

[22] M.-K. Seo, S.H. Kwon, H.S. Ee, and H.G. Park, "Full three-dimensional subwavelength high-Q surface-plasmon-polariton cavity," Nano Lett.9(12), 4078–4082 (2009)

[23] J. H Kang, Y. S No, S. H. Kwon, and H.-G. Park, "Ultrasmall subwavelength nanorod plasmonic cavity," Opt. Lett. 36(11), 2011–2013 (2011)

[24]C. Manolatou and F. Rana, "Subwavelength nanopatch cavities for semiconductor plasmon lasers," IEEE J. Quantum Electron. 44(5), 435–447 (2008).

[25] A. M. Lakhani, K. Yu, M. C. Wu, "Lasing in subwavelength semiconductor nanopatches," Semicond. Sci. Technol. 26(1), 014013 (2011)

[26] S.H. Kwon, "Deep subwavelength plasmonic whispering-gallery-mode cavity," Opt. Express 20(22), 24918–24924 (2012)

[27] E. Feigenbaum and M. Orenstein, "Optical 3D cavity modes below the diffraction-limit using slow-wave surface-plasmon-polaritons," Opt. Express 15, 2607-2612 (2007)

[28] Y. Song, J. Wang, M. Yan, and M. Qiu, "Subwavelength hybrid plasmonic nanodisk with high Q factor and Purcell factor," J. Opt. 13(7), 075001 (2011)

[29] S. W. Chang, T. R. Lin, and S. L. Chuang, "Theory of plasmonic fabry-perot nanolasers," Opt. Express 18(14), 15039–15053 (2010)

[30] Goebel, E. O. Luz, G. Schlosser, "Optical gain spectral of InGaAsP-InP double heterostructures", IEEE J. Quantum Electron.15, 697-700(1979)

48